



Atomistic simulations of dislocations and defects

JOHN A. MORIARTY^{a,*}, VACLAV VITEK^b, VASILY V. BULATOV^a and SIDNEY YIP^c

^a*Lawrence Livermore National Laboratory, University of California, Livermore, CA 94551, U.S.A.*

^b*Department of Materials Science and Engineering, University of Pennsylvania, Philadelphia, PA 19104, U.S.A.*

^c*Department of Nuclear Engineering, Massachusetts Institute of Technology, Cambridge, MA 02139 U.S.A.*

Abstract. This paper reviews selected recent research on the atomistic simulation of dislocation and defect properties of materials relevant to the multiscale modeling of plasticity and strength, with special emphasis on bcc metals and including work at extreme conditions. Current topics discussed include elasticity and ideal strength, dislocation structure and mobility, grain boundaries, point defects, and rapid resolidification, as well as noteworthy examples of research that directly impacts the issue of linking of length and/or time scales, as required in multiscale materials modeling. The work reviewed has been inspired by the recent international Workshop on Multiscale Modeling of Materials Strength and Failure held in October 2001 at Bodega Bay, California.

Keywords: Atomistic simulation, elasticity, dislocations, defects, multiscale modeling, plasticity, strength

1. Introduction

The predictive multiscale materials modeling of mechanical properties such as crystal plasticity and strength requires an in depth understanding and elaboration of fundamental defect and deformation processes at the atomic length scale as essential input into 3D microscale dislocation-dynamics [1] and other higher-length-scale simulations [2]. This demands the accurate atomistic modeling of the structure, motion and interaction of relevant point and extended defects, including vacancies, self-interstitials, impurities, dislocations and grain boundaries, as well as the accurate modeling of the relevant aspects of elasticity, including elastic moduli and the limits of elastic stability. To accomplish this task, we not only need to understand the underlying *qualitative mechanisms* that control plastic deformation, but we also need to be able to determine the *quantitative parameters* that will allow a predictive description of plasticity and strength properties in real materials under various conditions. The latter is particularly important in regimes where experimental data is scarce or nonexistent such as under the extreme conditions of pressure, temperature, strain and strain rate of interest to many modern applications, including the current Department-of-Energy (DOE) programs at the U.S. national laboratories.

Historically, the mechanical properties of materials have been classified and studied by crystal-structure type. In elemental materials, fcc, hcp and bcc metals, as well as diamond-cubic semiconductors, have all received significant attention in this regard and have become prototypes for different general types of mechanical behavior. In the context of current DOE programs such as ASCI (Accelerated Strategic Computing Initiative) [3], there has been special emphasis placed on understanding dislocation behavior and plastic deformation in bcc

*To whom correspondence should be addressed, E-mail: moriarty2@llnl.gov

transition metals, and this has helped to generate renewed research interest in these systems. Despite much improvement over the years in the description of interatomic interactions, general modeling methodologies and computer performance, much remains unknown at the atomistic level about the fundamental mechanisms and quantitative parameters of dislocation motion in these materials. The numerous papers published on this subject beginning in the 1960s, especially the classic ones by Vitek and Duesbery [4, 5], have identified many of the peculiar and distinguishing characteristics of dislocation behavior in bcc metals and have laid the groundwork for current investigations. Moreover, as has been observed by Duesbery, Vitek and others, bcc metals provide as much if not more insight into generic issues in crystal plasticity than do fcc metals and continue to be the *de facto* test bed for fundamental research. Consequently, a great deal of the discussion below centers on current research issues in bcc metals.

Whether studying bcc metals or any other class of materials, an important general consideration is the identification and separation of pure *generic* behavior representative of the materials class as a whole from *materials-specific* behavior representative of chemical differences or environmental factors such as high pressure. The historical perspective has been to assume that dislocation and grain-boundary behavior is highly generic for a given crystal class such as bcc. Evidence from recent quantum-based simulations and experimental measurements on bcc metals, however, suggests that this is not always the case, at least for some properties. In particular, the simulated core structure of screw dislocations [5–16] and the simulated and measured atomic structure of grain boundaries [17–23] have shown definite evidence of materials-specific behavior. This points to the importance of chemical bonding, in addition to crystal symmetry, in elaborating defect and deformation behavior. In bcc metals, chemical bonding ranges from non-directional, nearly-free-electron *sp* bonding in the alkali metals (e.g., Na, K) to directional *d*-electron bonding in transition metals (e.g., Ta, Mo, Fe). The latter also depends strongly on *d*-electron occupation, which varies considerably from nonmagnetic group-VB (e.g., Ta) and group-VIB (e.g., Mo) elements to magnetic group-VIII elements (i.e., Fe). One cannot automatically assume that behavior found for one material under very specific conditions is representative of the whole class under the same or more general conditions.

Large-scale computer simulation is at the heart of modern atomistic modeling and both the possibilities and the limitations of what can be accomplished in studying defect and deformation processes at the atomic scale is controlled by the specific computational methodologies available and the extent to which the simulations can be validated experimentally. Typically, an atomistic simulation is performed on a specified finite collection of atoms contained within a chosen computational cell of variable shape and size to which specific boundary conditions and other constraints such as temperature, stress and strain rate are applied. Both molecular statics (MS) techniques, which seek to minimize the total energy of the system at zero-temperature, and finite-temperature molecular dynamics (MD) techniques are widely used. For defect and deformation simulations, realistic boundary conditions represent a crucial ingredient to obtain meaningful results. For point defects and grain boundaries, some combination of fixed boundary conditions (FBC), where the exterior atoms are frozen at their bulk lattice positions, and periodic boundary conditions (PBC), where atomic positions are periodically replicated, are usually used. The latter often allow smaller simulation cells to be used and are prevalent in methods where cell size is an issue.

The atomistic simulation of individual dislocations requires special treatment due to the long-ranged ($\sim 1/r$) elastic field associated with them. Historically, FBC have been most

often used in such dislocation simulations, where distant atomic positions are established by the conditions of linear anisotropic elasticity. This requires very large simulation cells in practice, but this method is always problematic with respect to force build-up between fixed and relaxed atomic regions. An elegant and practical solution to the latter problem is to use so-called flexible boundary conditions. Rao *et al.* [24, 25] have recently developed an advanced Green's-function version of such conditions for both 2D and 3D dislocation simulations, denoted as Green's function boundary conditions (GFBC). In this method, a buffer layer is introduced between the fixed outer and inner relaxed atomistic regions of the simulation cell, allowing one to dynamically update the boundary conditions of the simulation, while dramatically reducing the size of the atomistic region. Periodic boundary conditions have also been used to treat two identical dislocations arranged in the form of a dipole (and also four identical dislocations arranged as a quadrupole). Here the distant $1/r$ monopole field is cancelled exactly, but a special problem arises due to the image effects associated with remaining long-ranged elastic interactions. This issue has been dealt with recently by Cai *et al.* [26] by the introduction of a method to calculate the anisotropic elastic energy of a dislocation dipole in a periodic cell, in which the infinite image summation is absolutely convergent. The method entails evaluating the reversible work to create an array of dislocation dipoles and allows the core energy of a dislocation to be extracted from an atomistic simulation in a manner that is manifestly system-size invariant. Additionally, they find that the energy barrier produced by the periodic boundary conditions can be effectively eliminated by the selection of an optimum aspect ratio of the simulation cell, a practical result that apparently has not been previously appreciated.

The second important ingredient needed in atomistic simulations is a set of interatomic forces that move the atoms and reflect the quantum-mechanical chemical bonding. These forces are most often obtained from corresponding *interatomic potentials*, which in turn have been developed to differing degrees of sophistication. In metals, empirical radial-force potentials of either the embedded-atom (EAM) type [27] or the Finnis-Sinclair (FS) type [28] are the forms most often used in large-scale MD simulations. While these potentials are attractive for their computational efficiency and convenience, they do not explicitly model the directional bonding in central transition metals. For such metals with partially-filled d -electron bands, however, quantum mechanics gives rise to non-radial forces and explicit angular-force contributions to the interatomic potentials [29–31]. In recent years, quantum-based interatomic potentials for transition metals that contain explicit angular-force contributions have been developed from tight-binding theory [31–33] as well as from first-principles generalized pseudopotential theory (GPT) [29], which is based on fundamental density functional theory (DFT) [34]. The former include Pettifor's bond-order potentials (BOPs) [31, 35, 36], while the latter include Moriarty's model-GPT or MGPT potentials [37–39]. Both MGPT and BOP potentials for bcc transition metals are now in a rather advanced development stage and are being actively applied to dislocations and other defect calculations. In addition, there have been several recent attempts to apply *ab initio* all-electron or pseudopotential DFT electronic-structure techniques directly to calculate point-defect energies [12, 40], grain-boundary atomic structure [21], and dislocation core structures and Peierls stress [10, 11, 16, 41]. These methods usually require very small computational cells and are subject to the same concerns about boundary conditions and other factors as are the atomistic simulations.

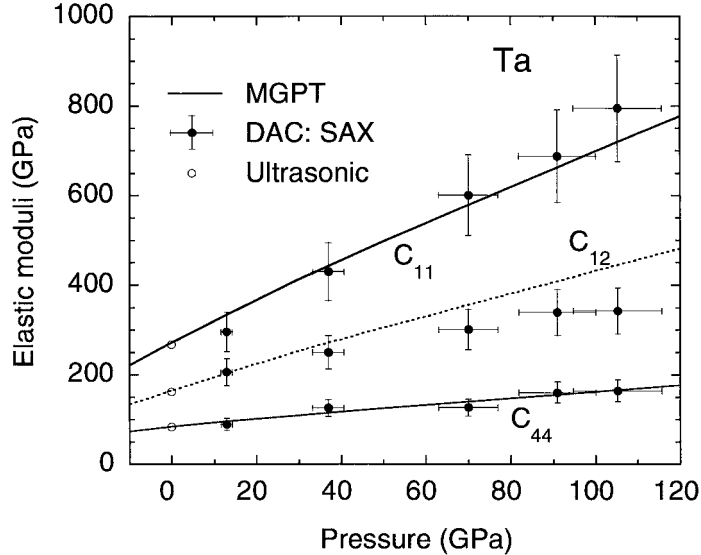


Figure 1. Comparison of calculated MGPT high-pressure elastic moduli in bcc Ta with recent measurements in the diamond-anvil cell (DAC) by the SAX technique to 105 GPa [44] and with ultrasonic data at ambient pressure [42].

2. Current research developments

In this section, we discuss selected recent and current research developments in the areas of elasticity and ideal strength, dislocation structure and mobility, grain boundaries, point defects, and rapid resolidification.

2.1. ELASTICITY AND IDEAL STRENGTH

The single-crystal elastic moduli of a solid are fundamental quantities that are essential to describing its mechanical behavior and often serve as basic constraints on interatomic potentials used in the atomistic simulation of dislocations and other defects. In addition, polycrystalline averages of these moduli performed as a function of pressure and temperature are frequently used to scale constitutive models of strength to extreme conditions, as discussed in Section 3.5. At ambient pressure, values of the single-crystal elastic moduli and their first pressure derivatives are well established in most bcc transition metals and other elemental materials through standard ultrasonic measurements (e.g., [42]). The best *ab initio* DFT electronic-structure methods can calculate these moduli to an accuracy of about 10% or better, and at high pressure, where experimental data are scarce, accurate all-electron DFT calculations are especially useful in this regard.

In the case of Ta, pressure-dependent elastic moduli $C_{ij}(P)$ have been so determined to 1000 GPa [43] and recently used to develop corresponding MGPT potentials [12, 39]. The calculated Ta shear moduli C_{44} and $C' = (C_{11} - C_{12})/2$ display rather smooth monotonic increases with pressure over this range, although interestingly, the corresponding anisotropy ratio, $A = C_{44}/C'$, displays a distinctive minimum near 150 GPa [39]. In Fig. 1, the individual calculated moduli, as obtained with the Ta MGPT potentials, are compared with recent diamond-anvil-cell measurements [44] to 105 GPa, as obtained with the so-called SAX technique described below in Section 4.1. The temperature dependence of elastic moduli is

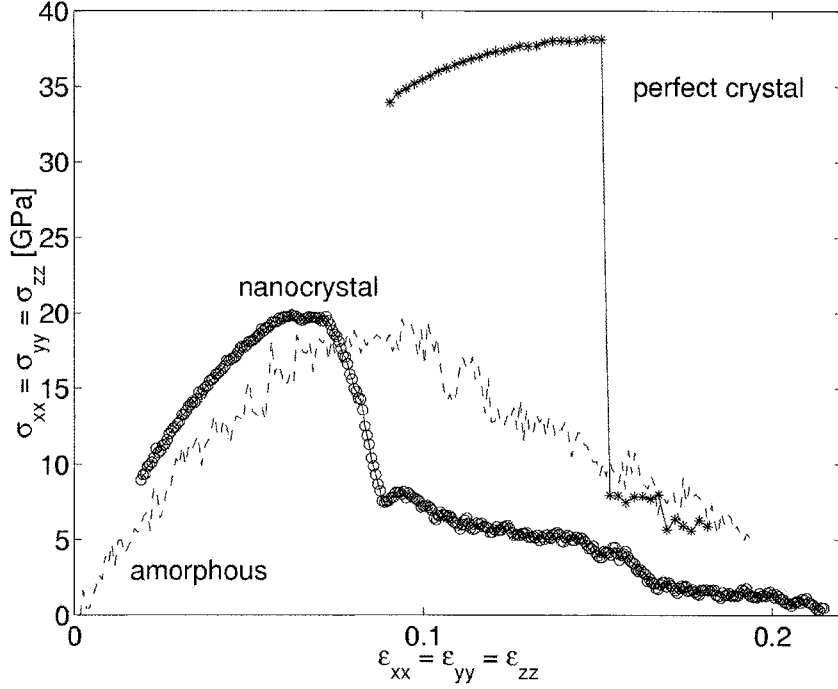


Figure 2. Variation of virial stress at constant strain from MD simulations of SiC (3C) under hydrostatic tension at 300 K in perfect-crystal, amorphous, and nanocrystalline phases.

similarly important in the context of mechanical properties, and there has also been recent theoretical work aimed at treating the high-temperature thermoelastic properties of bcc and other metals by including additional ion-thermal and electron-thermal contributions to the moduli [45–47].

More generally, the theoretical basis for describing the mechanical stability of a crystal lattice lies in the formulation of elastic stability conditions that specify the critical level of external stress that the system can withstand. Lattice stability is not only one of the most central issues in elasticity, it is also fundamental in any analysis of structural transitions in solids, such as polymorphism, amorphization, fracture, or melting. Born was the first to derive a set of conditions on the equilibrium elastic constants of the crystal that must be satisfied to maintain structural stability [48]. This has led to the determination of ideal strength of crystals as an instability phenomenon [49–51]. The extension of such elastic stability criteria to finite stress has been considered by a number of workers [e.g., 52–54] and is most simply expressed through the elastic stiffness tensor

$$B_{ijkl} = C_{ijkl} + \Lambda_{ijkl}, \quad (1)$$

where C_{ijkl} is the elastic-constant tensor and the tensor Λ_{ijkl} depends only on the applied stress component τ_{ij} . The usual conditions of elastic instability at zero stress, expressed by the vanishing of the lowest eigenvalue of C_{ijkl} , are then replaced at finite stress by similar conditions in terms of the B_{ijkl} . Under hydrostatic pressure P in cubic crystals, corresponding to a uniform expansion or compression of the lattice, the B_{ijkl} are readily interpreted as the pressure-dependent elastic moduli $C_{ij}(P)$ of the expanded or compressed solid, as discussed above.

The connection between stability criteria and theoretical strength is also straightforward. One can imagine the lattice being subjected to an increasing tensile or shear stress and evaluating the stiffness coefficients B_{ijkl} until a point of instability is reached. The critical stress at that point is then a measure of the theoretical strength of the solid. The validity of the stability criteria can be quite simply demonstrated by a direct MD simulation of the stress-strain response for a prescribed mode of deformation, as shown in Fig. 2 for samples of β -SiC under constant hydrostatic strain with periodic boundary conditions. At every step of the imposed strain, the system is relaxed via MD and the virial stress evaluated. The single-crystal sample shows the expected linear elastic response at small strain up to about 0.03; thereafter the response is nonlinear but still elastic up to the critical strain of 0.155 and corresponding stress of 38 GPa. This value of the critical strain is in agreement with what one obtains from the condition of $C_{11} + 2C_{12} + P = 0$, with P being the critical stress. After the onset of instability one finds by inspection of the resulting atomic configurations that the lattice has failed by the nucleation of a nanocrack; this result could not have been predicted on the basis of the stability criteria. The response curves for the nanocrystalline and amorphous samples show characteristically different features, a marked reduction of strength, by a factor of about 2, and the absence of a sharp transition when the systems start to yield. This contrast is noteworthy in demonstrating in a simple manner the effects of defect microstructure on strength. Thus the perfect crystal response is ideal in that no defects of any kind are present in the initial state; the system exhibits maximum (theoretical) or upper limit to strength. It also should be clear that different stability criteria will lead to different determinations (and therefore definitions) of strength. An extension of elastic instability is vibrational instability as measured by soft phonon modes which can occur away from the Brillouin zone center for certain lattices and modes of deformation [55].

In the case of bcc metals, there have been a number of recent studies of ideal shear strength τ_c at ambient as well as extreme conditions of pressure using both DFT electronic-structure methods and quantum-based interatomic potentials [8, 12, 43, 56–58]. These studies have shed light on correlations of the ideal strength with the corresponding shear modulus G , with deformation geometry, and with pressure. For $\langle 111 \rangle$ loading, τ_c generally scales linearly with $G_{111} = (2C' + C_{44})/3$ and does not seem to be sensitive to either the particular shear plane chosen or to atomic relaxation effects. In the case of Ta, the high-pressure ideal shear strength has been calculated to 1000 GPa, with all-electron DFT and quantum-based MGPT results in good agreement. This provides a useful validation test on the MGPT potentials for large deformations. In addition, with the MGPT Ta results it is found that to a good approximation the scaling relation $\tau_c(P) = 0.12G_{111}(P)$ holds over the entire 0–1000 GPa pressure range.

2.2. DISLOCATION STRUCTURE AND MOBILITY

The low-temperature and high-strain-rate plasticity of bcc metals is largely controlled by the intrinsic core properties of $a/2\langle 111 \rangle$ screw dislocations. Unlike the highly mobile edge dislocations in these metals, the motion of the screw dislocations is severely restricted by the non-planar atomic structure of its core, resulting in low mobility, thermal-activated kink mechanisms, and a temperature-dependent yield stress.

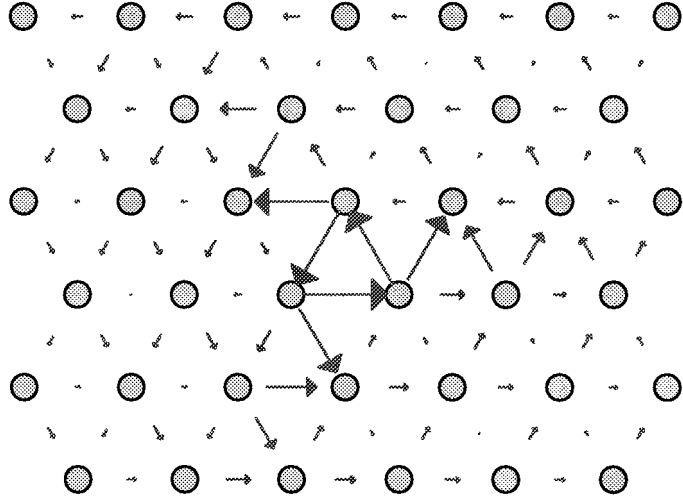


Figure 3. Differential displacement map of the equilibrium core structure of the $a/2\langle 111 \rangle$ screw dislocation in bcc Mo calculated with a FS potential and FBC [59]. This result is representative of a three-fold-spread, degenerate core structure in bcc metals.

2.2.1. Ground-state core structure and energy

The stable ground-state core configuration of the $a/2\langle 111 \rangle$ screw dislocation is centered among three $\langle 111 \rangle$ atomic rows forming a triangular prism. Around these three rows the near-neighbor atoms are positioned on a helix that winds up in a clockwise or counter-clockwise manner, depending on the location of the elastic center and the sign of the Burgers vector \mathbf{b} . In general, the ground-state core can exhibit a three-fold directional spreading, of variable magnitude, along three $\langle 112 \rangle$ directions on three $\{110\}$ planes of the $\langle 111 \rangle$ zone. This can happen in two geometrically distinct but energetically equivalent ways, resulting in a doubly degenerate core structure with the two possible core configurations related by the $\langle 110 \rangle$ diad. Under the right circumstances, however, the spreading may vanish and the two configurations become identical, yielding a single isotropic and non-degenerate core structure with a higher, but still three-fold, symmetry. The fact that different core structures are thus possible in bcc metals has made its prediction an interesting *materials-specific* point of comparison among the various computational methods, where the result obtained can depend sensitively on interatomic forces, boundary conditions, and external environment. Examples of calculated three-fold-spread [59] and isotropic [14, 15] equilibrium core structures are displayed in Figs. 3 and 4, respectively, using the standard differential-displacement scheme of Vitek [4]. In this scheme, the $\langle 111 \rangle$ screw components of the relative displacement of neighboring atoms due to the dislocation is represented by an arrow between the two atoms. Corresponding maps can also be constructed for the perpendicular edge components of the dislocation as well, but these are much smaller in magnitude [5, 11, 12].

Early model studies of core structure using empirical pair potentials and FBC [4, 60] yielded three-fold-spread, degenerate structures, and for many years this was widely assumed to be the generic result for bcc metals. Subsequent calculations with quantum-based potentials confirmed this picture, first in K using a first-principles pseudopotential-derived pair potential and FBC [6, 7, 61] and then in Mo using early (1994) MGPT many-body potentials with FBC [8] and later with GFBC [9]. In 1998 Duesbery and Vitek [5] reported the first systematic study of the equilibrium core structure in the group-VB and -VIB bcc transition metals based on em-

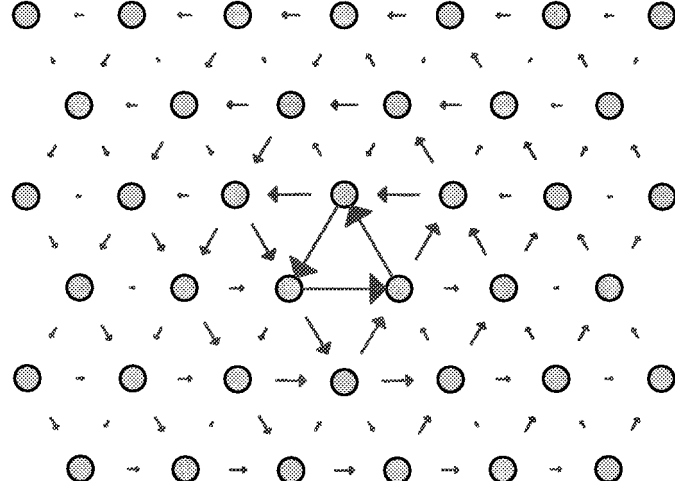


Figure 4. Differential displacement map of the equilibrium core structure of the $a/2\langle 111 \rangle$ screw dislocation in Mo from BOP atomistic calculations with FBC [14, 15]. This result is representative of an isotropic, non-degenerate core structure in bcc metals.

pirical FS potentials and FBC. They too obtained three-fold-spread, degenerate structures for the group-VIB metals (Cr, Mo, W), but in contrast, they predicted isotropic, non-degenerate structures for the group-VB elements (V, Nb, Ta). The same compact isotropic core structure for both Ta and Mo was also obtained by Ismail-Beigi and Arias [10] in the first direct DFT dislocation calculation on bcc metals. In the latter approach, a quadrupolar arrangement of four dislocation cores in a small computational cell containing only 90 atoms with PBC was considered. Recently, Woodward and Rao [11] have confirmed these latter results using an adaptation of the GFBC method to DFT electronic-structure calculations, as have Sadigh *et al.* [16] in Mo using DFT calculations with improved PBC. In addition, such calculations provide some additional insight on the nature of chemical bonding in the dislocation cores through detailed elaboration of the electron density, as illustrated for Mo in Fig. 5. At the same time, recent atomistic simulations in Ta and Mo with new optimized MGPT potentials and GFBC [12, 13] and in Mo with new screened BOP potentials and FBC [14, 15] also support an isotropic equilibrium core structure in these metals.

Equally revealing is the volume or pressure dependence of the core structure, which has now been explored in the cases of Ta and Mo via MGPT simulations [12, 13]. This dependence is usefully quantified by the so-called polarization p of the degenerate core, which measures the simultaneous translation of the three central atoms nearest to the core center. This translation is parallel to the dislocation line but in the opposite sense for the two different core orientations (commonly denoted as positive p and negative n). When p vanishes, the two core configurations coincide and an isotropic core structure is obtained. At $p = \pm b/6$, on the other hand, a fully polarized core is obtained with maximum three-fold spreading along $\langle 112 \rangle$ directions. In Fig. 6, the calculated magnitude of the core polarization in Ta is plotted as a function of volume and hydrostatic pressure. Near equilibrium and at expanded volumes (i.e., negative pressure), the polarization becomes negligibly small ($< 0.01b/6$) and is zero within the numerical precision of the calculations, thus corresponding to an isotropic core. Under compression, however, the polarization grows rapidly, so that at high-pressure the core assumes a clear three-fold-spread structure. A similar result has now also been obtained in the

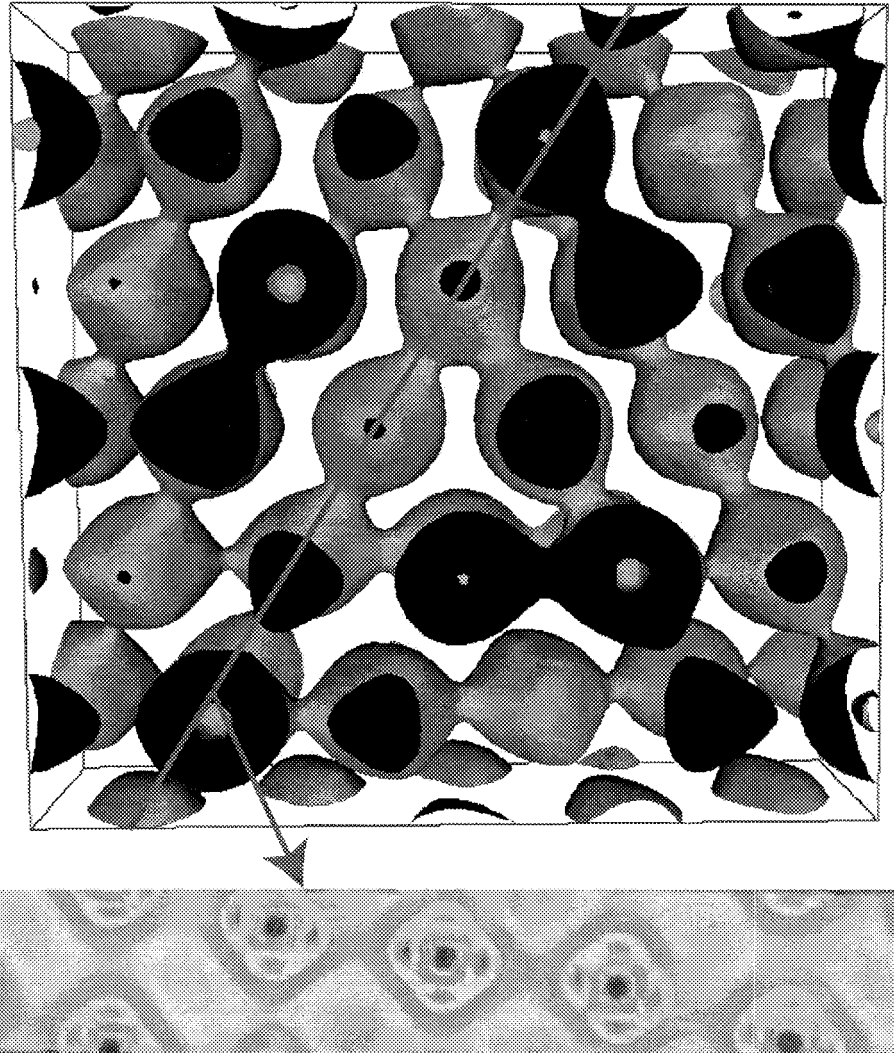


Figure 5. Isosurface electron-density plot of the region near the dislocation core in bcc Mo obtained from an *ab initio* DFT calculation with flexible GFBC [11]. The inset shows a cross-section of the electron density in a {110} plane adjacent to the dislocation core.

case of Mo [13]. In addition, these results clearly show that the transition from a spread to an isotropic core is a continuous one and definitely not akin to a first-order phase transition.

Significant effort has also been spent on computing core energies. While this can provide useful estimates of the core size and other internal checks [8, 12], in most situations of practical importance, the core contribution to dislocation interaction energetics is considerably smaller than the corresponding elastic-energy contribution. This ratio, however, may change significantly when it comes to the energetics of dense dislocation groups. In particular, values of the core energy become more significant when compared among dislocations of different character. Cai [62] has recently found, similar to an earlier result obtained for dislocations in Si, that the core energy as a function of dislocation character shows behavior fundamentally similar to the dependence of the grain boundary energy on the misorientation angles. In par-

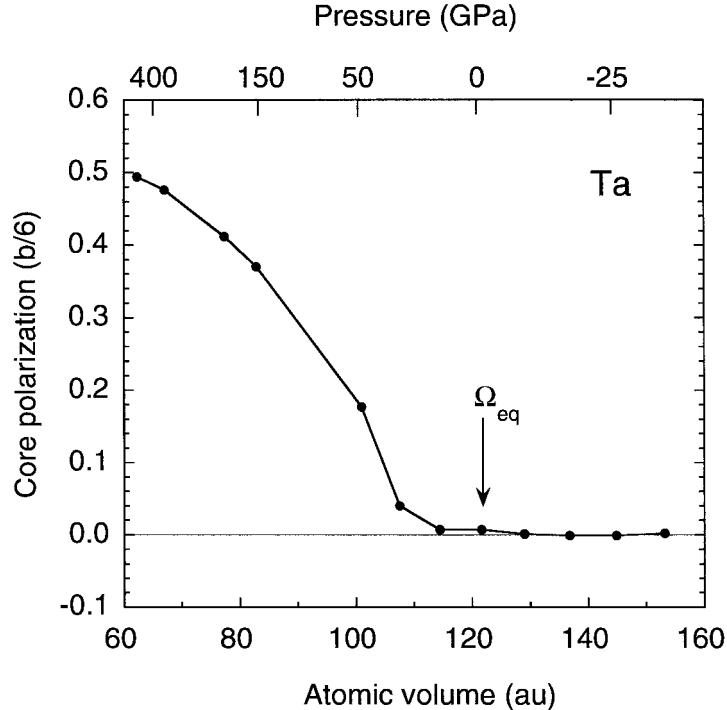


Figure 6. Volume and hydrostatic pressure dependence of the $a/2(111)$ screw dislocation core polarization in bcc Ta, as calculated with MGPT interatomic potentials and flexible GFBC (solid points) [13]. Near equilibrium (Ω_{eq}) and at expanded volumes the core polarization is less than $0.01b/6$ consistent with an isotropic, non-degenerate core.

ticular, for $a/2(111)$ dislocations in $\{110\}$ planes of bcc Mo (as modeled by a FS potential), cusp-like features are observed on the core energy-versus character-angle curve. Specifically, a cusp is clearly seen centered on the special 71° orientation (denoted as the M111 dislocation by Yamaguchi and Vitek [63]). Although by itself the depth of this cusp is small and probably too insignificant to define any observable feature in the dislocation microstructure, the very appearance of a cusp may signal something important about the dislocation mobility, as discussed below. As will also be explained below, such a connection between core energies and mobilities is not accidental but reflects a common origin of the two parameters. This connection also calls for more calculations of the core energies as a function of the generalized dislocation character discussed in Section 2.2.4.

2.2.2. Kink-pair formation and migration

At finite temperature, the motion of the screw dislocations in the bcc lattice normally occurs by the thermally assisted formation and migration of kink pairs. For low-stress conditions, the individual kinks in a kink pair are well separated and weakly interacting, so kink-pair formation can be studied by just looking at isolated kink formation. In this limit, the nature and atomic structure of the possible kinks is closely related to the unstressed dislocation core. At any polarization p , the doubly-degenerate core structure results in different possible kinks and kink-pair configurations involving p and n segments that can be formed. In addition, p and n segments can co-exist on the same dislocation line in the form of a so-called anti-phase defect (APD). In general, two different anti-phase defects on the dislocation line (np and pn)

and six distinct and non-degenerate kinks are geometrically possible [64]. Only kinks formed on {110} planes are normally modeled in bcc metals, as kinks formed on other planes such as {211} have significantly larger kink heights and formation energies and are usually found to be unstable in atomistic simulations [65]. Duesbery has further shown in Mo that kink pairs formed on {211} planes spontaneously disintegrate into kink pairs on {110} planes [66]. This is in sharp contrast to the strong claims made by Seeger *et al.*, based on detailed flow stress measurements with high-purity single crystals, that screw dislocation motion in Mo should take place via kink formation on {211} planes [67]. This discrepancy needs to be resolved and would warrant appropriate atomistic study of kink formation under stress in Mo as well as a more fundamental analysis of the Seeger *et al.* data.

In the case of Ta, the atomic structures and formation energies of the possible APDs, isolated kinks, and kink pairs in Ta have been calculated and elaborated in detail using optimized MGPT potentials and GFBC [12]. The lowest energy kink pair that can be formed from isolated left and right kinks without a pre-existing APD has a formation energy of 0.96 eV. This value is in close agreement with the empirical zero-stress activation enthalpy of 1.02 eV currently used in microscale dislocation-dynamics simulations to model the temperature-dependent yield stress and plastic flow in bcc Ta [68]. For this kink pair, the related issue of kink migration, which is limited by the secondary Peierls stresses needed to move the left- and right-hand kinks, has also been investigated. These secondary stresses are calculated to be 1–2 orders of magnitude smaller than the corresponding Peierls stress for the rigid screw dislocation itself (see below), so both kinks are expected to be mobile. Consequently, the dislocation velocity at low stress should be controlled by kink-pair formation rather than kink migration.

At smaller finite separation, the left and right kinks will elastically attract each other, requiring an applied shear stress to maintain the separation. For low levels of stress, the activation enthalpy for the balanced kink pair can be calculated directly in terms of the total formation energy of the kink pair under the applied stress, which can be obtained from direct MS simulations. At higher levels of stress, however, special methods must be applied that allow the dislocation line itself to move and begin to climb the Peierls barrier in a self-consistent manner [69]. In the case of Ta with MGPT potentials and GFBC, the stress-dependent activation enthalpy has been so calculated at both ambient and extreme conditions of pressure [12, 13, 69]. These results have been used in turn to model dislocation mobility for use in dislocation-dynamics simulations, as discussed in Section 3.2.1.

Another interesting development in this area is the Edagawa *et al.* continuum model of kink pairs under stress [70]. Similar to the classic Peierls-Nabarro model, it replaces a fully atomistic description with a much less detailed continuum framework that incorporates limited atomistic data in the form of a misfit potential. However, the nature of this potential reflects the bcc lattice geometry much better than the Peierls-Nabarro model that implies an fcc-like confinement of screw dislocations to the glide planes. Edagawa's model provides a basis for development of an accurate theory of kinks on screw dislocations in bcc metals that can meaningfully utilize accurate *ab initio* DFT energetics. It appears possible to develop such an approach within the computational limitations of DFT.

2.2.3. Peierls stress

To complete the double-kink mobility model in bcc metals, one must also consider the high-stress, low-temperature limit. A very fundamental issue in this regard is the magnitude and orientation dependence of the lattice-friction or Peierls stress to move the rigid straight screw

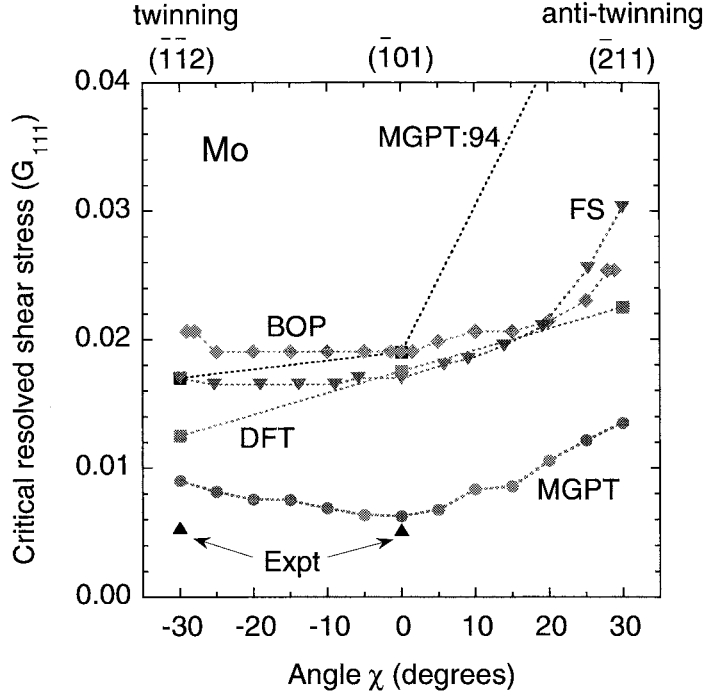


Figure 7. Critical resolved shear stress (CRSS) and its orientation dependence in Mo, as calculated with BOP [14, 15] and FS [59] potentials, using FBC, and with MGPT (1994) potentials [9], new MGPT potentials [13], and an *ab initio* DFT method [11], all using flexible GFBC.

dislocation at zero temperature. The Peierls stress controls the yield stress of the material at low temperatures, and in particular, is responsible for the well known observed deviations from ideal Schmid-law slip behavior that are characteristic of bcc metals [5, 59, 72–75]. In these metals, slip predominantly takes place in {110} or {112} planes at low temperatures. In a bcc crystal along a given ⟨111⟩ direction, there are three {110} planes and three {112} planes, mutually intersecting every 30°. Unique values of the critical resolved shear stress (CRSS) to initiate dislocation motion can exist on different maximum resolved shear-stress (MRSS) planes ranging in orientation from $\chi = -30^\circ$ (twinning orientation on {211}) to $\chi = +30^\circ$ (anti-twinning orientation on {211}), with χ being the angle measured from a given {110} slip plane. If the dominant slip plane is {110}, as in the case of Mo, the Schmid law implies that the CRSS should vary as $1/\cos(\chi)$, whereas if the dominant slip plane is {112}, as is the case in Ta, then one expects the CRSS to vary as $1/\cos(\chi + 30^\circ)$ [59]. Deviations from these expectations are said to represent non-Schmid behavior.

The Peierls stress and its orientation dependence under a pure shear stress applied in the ⟨111⟩ direction have been investigated through atomistic modeling by a number of workers in both Mo and Ta. Recent results of such calculations in Mo that employed a central-force FS potential with FBC [59], new many-body screened BOPs with FBC [14, 15], both 1994 [9] and new [13] many-body MGPT potentials with GFBC, and a DFT electronic-structure method [11, 41] also with GFBC are summarized in Fig. 7. Although there are clear quantitative differences, the calculated dependence of the CRSS on the angle χ is qualitatively similar in all five calculations with a substantial twining–anti-twinning asymmetry in each case that is characteristic of non-Schmid behavior. For $\chi < 0$, when the nearest {211} plane is sheared in

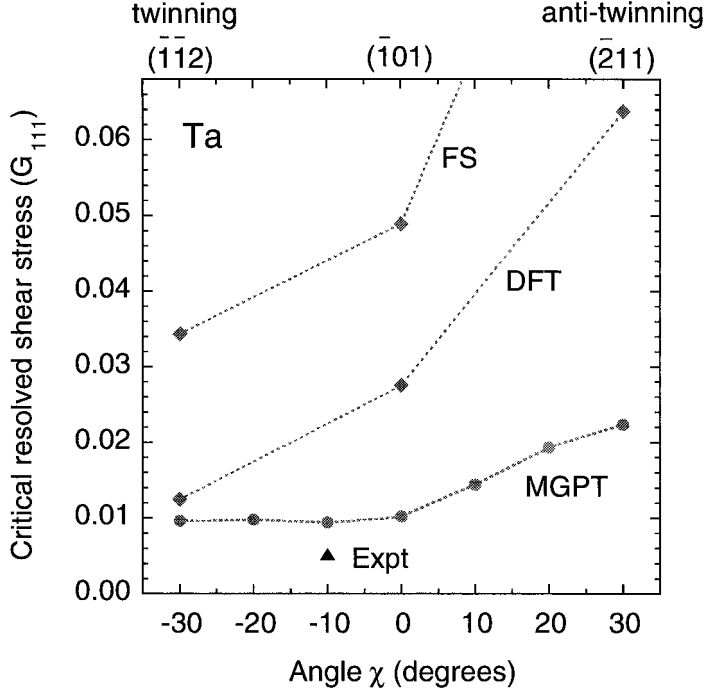


Figure 8. Critical resolved shear stress (CRSS) and its orientation dependence in Ta, as calculated with a FS potential [59], using FBC, and with MGPT potentials [12] and an *ab initio* DFT method [11], both using flexible GFBC.

the twinning sense, the CRSS tends to be rather constant, while it increases more rapidly for $\chi > 0$, when the nearest {211} plane is sheared in the anti-twinning sense. Furthermore, in the cases studied, the dislocation is found to glide along the most highly stressed {110} plane for any value of χ . This suggests that the symmetry of equilibrium dislocation core structure, which is isotropic in three cases but three-fold spread in the other two cases, does not play a decisive role in the glide properties, i.e., the Peierls stress and preferred slip plane, of the $a/2\langle 111 \rangle$ screw dislocations. More likely, the deciding factor is the way the core transforms under the influence of the applied stress. Indeed, a screened-BOP core calculated at an applied stress level just before the movement starts for $\chi = 0^\circ$ loses its isotropic character and becomes more akin to the three-fold-spread configuration shown in Fig. 3 [14, 15].

In the case of Ta, similar Peierls-stress calculations employing a central-force FS potential with FBC [59], many-body MGPT potentials with GFBC [12], and a DFT electronic-structure method with GFBC [11, 41] are shown in Fig. 8. The dependence of the CRSS on χ reveal significant non-Schmid behavior in each case with the twinning–anti-twinning asymmetry even more pronounced than in Mo. However, unlike in Mo, the dislocation tends to glide along the {112} plane sheared in the twinning sense, typically via zig-zag atomic motion on successive {110} planes. Again it is not the equilibrium dislocation core structure, which is predicted to be isotropic in all three cases, but the changes induced by the applied stress that likely control the gliding of the $a/2\langle 111 \rangle$ screw dislocations.

Another important issue is the calculated quantitative magnitude of the Peierls stress τ_P , which, like the core structure itself, can depend sensitively on interatomic forces, boundary conditions and external environment. Experimentally in bcc metals, the Peierls stress is typ-

ically estimated to be about 0.5% of the $\langle 111 \rangle$ shear modulus G_{111} , a result obtained, for example, by extrapolating the observed low-temperature, single-crystal yield stress to zero temperature. This is indeed the case in both Mo and Ta [67, 68, 76, 77]. As seen in Figs. 7 and 8, most of the calculated CRSS curves are well above the experimental estimates of τ_P . One exception is the very recent result obtained in Mo with the new many-body MGPT potentials and GFBC, a result which closely approaches experiment near $\chi = 0^\circ$. In the case of Ta, on the other hand, the calculated MGPT CRSS for $\chi < 0$ is about a factor of two larger than experiment, as is the DFT result at $\chi = -30^\circ$. In this regard, the historical tendency for atomistic calculations to overestimate the Peierls stress has led to some recent speculation about possible missing physics. For example, the usual 2D zero-temperature calculation of the Peierls stress could possibly miss very low energy 3D and/or dynamic kink-like processes that might be activated in low-temperature experiments and could lead to an effectively lower estimated value of τ_P . Such a mechanism has been argued to be possible in the case of edge dislocations for bcc metals [78]. However, 3D finite-temperature MD simulations performed to investigate this possibility for $a/2 \langle 111 \rangle$ screw dislocations in Ta have found no evidence to support such a mechanism [79]. There is also the possibility that under certain circumstances collective dislocation motion can occur below the Peierls stress for an individual dislocation, as further discussed in Section 2.2.6 below.

A further important issue here is the pressure dependence of the Peierls stress $\tau_P(P)$. This has been investigated with many-body MGPT potentials and GFBC to 400 GPa in Mo at $\chi = -30^\circ$, 0° and $+30^\circ$ and to 1000 GPa in Ta at $\chi = 0^\circ$ [13]. The Mo results reveal that the quantitative degree of non-Schmid character can depend significantly on environmental factors such as pressure. The Ta results display a linear scaling with the shear modulus G_{111} similar to that found for ideal shear strength. In this case, it is found that $\tau_P(P) \cong 0.01G_{111}$. This is consistent with the assumptions made in some constitutive models of strength, as discussed in Section 3.5.

2.2.4. Edge and general character dislocations

It is a common perception in bcc metals that it is most important to understand and quantify the mechanisms of screw dislocation motion, and that other, non-screw components of the dislocation population are less important. While it appears likely that the overall rate of plastic strain is indeed controlled by the slow moving screws, behavior of the faster edge and mixed dislocations is not unimportant. This is because, as the microscale dislocation-dynamics (DD) simulations show (e.g., Tang *et al.* [68]), non-screw dislocations contribute as much to the net plastic strain as the screws. At the same time, since screw dislocations in bcc systems are totally free to glide in any plane of the $\langle 111 \rangle$ zone, for as long as the driving stress is high enough, non-screw dislocations should follow the screws into various planes, making it necessary to quantify their mobility in the planes other than $\{110\}$. It appears that, for the bcc systems, it is important to relate dislocation mobility to the dislocation character. The latter is commonly understood as the angle between the dislocation line and its Burgers vector which for the bcc metals are invariably thought to lie in the $\{110\}$ planes (only rarely are the $\{112\}$ planes considered). It is more informative and indeed necessary to examine dislocation mobility as a function of, what can be called, *generalized character*. This is defined by two angles. The first is a familiar angle between the Burgers vector and the dislocation line and the second is an angle between the glide plane (defined by the Burgers vector and the line-tangent vector) and a reference plane in the zone of the Burgers vector. Calculations for Mo ([80], using a FS potential) indicate that this notion of generalized character is fundamental to the

behavior of dislocations in bcc metals and must be included in any general implementations of DD codes for these materials. It is also observed that, contrary to the common prejudice, non-screw dislocations can behave very differently, depending on the exact values of the generalized character angles. For example, the Peierls stress of non-screw dislocations in a {110} plane varies by a factor of 16 (!) in an angular range of just 20 degrees. Despite such wide variations, one can identify rather simple and appealing arguments by which such interesting behaviors can be rationalized on the basis of the underlying lattice geometry. Furthermore, it can be shown that dislocation mobility is closely related to the corresponding variations of the core energy, both considered as functions of the generalized character.

2.2.5. Mobility at high stress and phonon drag

The direct observation of dislocation mobility by MD is not a straightforward task, as may be seen from previous attempts to activate dislocation motion in Si [81]. A key consideration is the intrinsic mobility of the dislocation, which involves knowledge of the activation energy barrier [82] or the Peierls-Nabarro stress [55, 83, 84]. In the case of bcc Mo, it is known that edge dislocations have considerably higher mobility than screws. MD results on edges obtained using a FS potential have been reported [85, 86] in the regime of high stress (above 10^2 MPa) and high velocity (10^2 m/s), giving the first glimpses of how a nanometer sized, straight dislocation segment actually glides through the lattice under an applied shear over distance of a few Burgers vectors in picosecond time periods. In this regime the dislocation velocity increases linearly with stress, and decreases with increasing temperature that is indicative of phonon drag. On the other hand, available data exist only in the low-stress (10 MPa) and low velocity (10^{-2} m/s) regime, showing a stress exponent of about 8. A crossover from kink-pair thermal activation to phonon drag behavior is known, for example in KBr, but this remains to be demonstrated in Mo or other bcc metals.

Calculations of dislocation mobility under high stress (close to or above the Peierls stress) have become commonplace. Beginning with Rodney and Martin [87], several groups observed that dislocation velocity is bounded by a terminal value, below the longitudinal but above the transverse sound velocities. A few results obtained so far indicate that supersonic motion of dislocations can be achieved in direct MD simulations. Possibly the most detailed study of this issue is reported by Chang [88], who suggests that supersonic motion can only be achieved if a dislocation is driven hard in small, confined volumes, which is typical of the small cells used in most MD simulations. However, in larger cells, dislocation velocity reaches a terminal value and never ventures above the sound barrier, under the same loading conditions when a supersonic motion is observed in the smaller cells. This indicates that the issue of subsonic/supersonic dislocation motion is subtle and requires more work. Nevertheless, it appears possible, with some care, to quantify the phonon drag resistance by direct atomistic simulations using empirical interatomic potentials. Although this may not be sufficiently accurate to represent the real metal, more importantly one can verify the existing theory (e.g., Altshitz-Indenbom) for a given model material and, if the comparison is found accurate, apply the theory to real metals. A very interesting venue for further study would be to do such simulation-theory comparisons for dislocation motion under hydrostatic pressure. Here, recent work by Wolfer [89] provides more theoretical guidance.

2.2.6. Dislocation-dislocation interactions and cooperative mechanisms of motion

In a series of direct atomistic simulations for bcc Mo using a FS potential, Bulatov and Cai [90] have detected a strong effect of junction nodes on the dislocation mobility of a pure-screw dislocation network. Specifically, planar junction networks formed in the {110} planes of the bcc lattice are considered, in which all dislocations are of screw character and thus do not contribute any geometric (glide) constraints to the motion of other participating dislocations. The critical stress to move the network was obtained for different stress orientations and found to be always smaller ($\sim 50\%$) than that needed for an isolated screw dislocation. This effect is significant because it shows that junctions can enhance dislocation mobility rather than always diminish it as is conventionally thought. Such cooperative effects are traced to the details of atomic motion in and around the junction nodes, i.e., the singular zero-dimensional objects in which two dislocations join to form a junction. These observations may put to rest a dispute about possible effects of junctions on dislocation motion conjectured earlier to explain anomalous slip behavior in bcc transition metals [91]. The new results indeed show that dislocation networks formed in the {110} planes have enhanced mobility, but the observed atomistic mechanisms differ significantly from the earlier hypothesis. More generally, these results indicate that dislocation mobility may be significantly altered by interaction with other dislocations, which in turn could affect the interpretation of any experimentally determined Peierls stress. In the considered example, the apparent Peierls stress observed for the material would be lower than the true Peierls stress for an individual screw dislocation. In addition, such a dislocation interaction would provide a mechanism of cooperative slip on two or more slip systems that can possibly explain some of the recently observed slip anomalies at room temperature in Mo [92].

2.2.7. Cross slip

As was noted recently by Duesbery and Vitek [5], much of the prevailing thinking about dislocation mechanisms is still dominated by the fundamental insights gained in the 1950s and 60s into the physics of crystal plasticity in fcc metals. Yet, it is likely that fcc and fcc-like behaviors are not so common, but rather are somewhat exceptional. Cross-slip is a good example where the conventional notion of a special significance of the glide planes affects the way we think about dislocation motion in general. In fcc systems, because of the planar dissociation into the Shockley partials, dislocations are confined to {111} planes in which the dissociation takes place. Even if a dislocation is locally in a screw orientation, the planar dissociation confines it to move in the dissociation plane. Only relatively rarely some special event (cross-slip) takes place by which a dissociated screw dislocation constricts in the initial plane and then re-dissociates in the cross-slip plane. In fact, in Al where the stacking fault energy is high and dissociation is suppressed, the confining effect of the {111} planes is greatly diminished and slip in planes other than {111} is routinely observed. In bcc metals, where no intrinsic stacking faults exist, there is no reason for a screw dislocation to be confined to any particular plane. In this case, the selection of the glide plane is a compromise between the maximum-resolved-shear-stress (MRSS) plane and a close-by plane of low resistance to dislocation motion, in the {111} zone. As such, cross-slip events are indistinguishable from slip events – there is no need for any special mechanism, like constriction, i.e., re-dissociation taking place via the Friedel-Escaig mechanism in fcc metals, to allow the dislocation to change its motion plane. In this sense, the notion of glide planes for the bcc metals may need to be re-considered.

2.3. GRAIN BOUNDARIES

Understanding the properties of grain boundaries and their interaction with dislocations and other lattice defects are matters of intrinsic importance to the multiscale modeling of strength and failure in polycrystalline materials. The prediction of grain-boundary atomic structure also represents an important validation test for interatomic potentials because this is the one example of an extended defect where direct comparison with experiment is possible.

2.3.1. *Atomic structure*

In this section, we briefly discuss recent atomistic simulations and experimental measurements on the Σ_5 (310)/[001] symmetric tilt boundary in prototype bcc transition metals, including Nb [17, 21, 22], Mo [18, 19, 21, 22], and Ta [20, 21]. This particular grain boundary (GB) is of special interest for several reasons. First, it has been possible to fabricate high-quality bicrystals for this orientation and to study them experimentally using high-resolution transmission electron microscopy (HREM) [17–20, 23]. (Additional details about these experiments are discussed below in Section 4.2.) Second, the distributions of bond lengths and bond angles at this boundary are similar to those occurring in the vicinity of a bulk $a/2\langle 111 \rangle$ screw dislocation [39], so important aspects of the interatomic forces are being tested. Finally, the actual atomic structure of the grain boundary is not a generic feature of bcc metals, but rather is material dependent and is a sensitive test of the angular forces, which are found to be essential to a predictive description [17, 22].

The first atomistic simulations on Σ_5 (310)/[001] grain boundary in Nb were performed with a Monte Carlo method [17] using both angular-force MGPT potentials and radial-force EAM potentials. Subsequent MGPT studies have used MD combined with a simulated annealing technique [19, 20, 22], successfully employing both large simulation cells (up to 1960 atoms), with periodic boundary conditions in the GB plane and fixed boundary conditions along the [310] GB normal [19], as well as much smaller periodic cells [20, 22]. In a comprehensive study on Nb and Mo [22], small-cell MGPT results were also compared to parallel calculations with a DFT electronic-structure method [21], two separate tight-binding methods, and both BOP and FS potentials. The important structural issues for the Σ_5 (310)/[001] grain boundary are whether or not mirror symmetry is preserved across the boundary, and if not, what the magnitude of the relative atomic displacement along the [001] tilt axis is. For Nb and Mo, both the DFT calculations [21] and the MGPT [17, 19] and BOP [22] potentials correctly predict mirror symmetry in the case of Nb and the breaking of that symmetry in the case of Mo, with [001] displacements consistent with experiment. For Ta, where the mirror symmetry is observed to be broken as in Mo, the [001] atomic displacement is also quantitatively predicted with the MGPT potentials [20]. In this case, however, the DFT calculations of Ochs *et al.* [21] predict a mirror symmetric GB as in Nb. The reason for the latter discrepancy is not clear, but we note that unlike Nb and Mo, Ta is a heavy relativistic metal, a fact that is taken into account in the MGPT Ta potentials [39] but not in the DFT calculations [21].

2.3.2. *Dislocation-grain boundary interactions*

The interaction of dislocations with grain boundaries is a very important but not well-explored aspect of the physics of crystal plasticity. In fcc metals and ordered L_{12} alloys, there have been atomistic studies of the special case where the dislocation line is parallel to the grain boundary [93–95]. More recently, realistic 3D atomistic simulations of dislocation-grain boundary interactions have been performed by Miller and Abraham [96] on the symmetric pure tilt

boundaries in fcc Ni. Based on their observations, de Koning *et al.* [97] examined the resistance to the glide of lattice dislocations between adjacent crystal grains associated with a grain boundary. Using a combination of molecular dynamics (MD) simulations and a line-tension (LT) model they identified the geometrical parameters that are relevant in the description of this process. In the MD simulations of Miller and Abraham, they observed slip transmission of dislocation loops nucleated from a crack tip near a series of pure tilt GBs in Ni. The observations can be rationalised in terms of a LT model for the activation of a Frank-Read source in the presence of a GB. They find that the slip transmission resistance is a function of only three variables: (1) the ratio of resolved stresses on the incoming and outgoing slip systems, (2) the magnitude of any residual Burgers vector content left in the GB, and (3) the angle between the traces of the incoming and outgoing slip planes in the GB plane. Comparison with the MD simulations and experimental data shows that the LT model captures the essential energetics of slip transmission and suggests relatively simple functional relationships between the GB geometry and loading conditions on one hand and slip transmission resistance on the other.

In other work, the deformation behavior of nanocrystalline fcc metals simulated by MD have been recently reported, providing atomic-level details of the nucleation of Shockley partial dislocations from grain boundaries and their subsequent interactions [98]. It is known from the study of coarse-grained fcc metals that the common low-temperature mechanism of plastic deformation involves the continuous nucleation of dislocations from Frank-Read sources [99]. Since the stress needed for a source to operate is inversely proportional to its size, this mechanism is effective only down to a grain size of about $1\text{ }\mu\text{m}$. A competing mechanism that is expected to be important in nanocrystals is nucleation from grain boundaries. With the dislocation cores usually split into Shockley partials, whose separation distance depends on the stacking-fault energy and the applied stress, another length scale enters into the problem since the equilibrium separation between partials can be comparable to or larger than the grain size in a nanocrystal. Dislocation activity in a nanocrystal undergoing tensile deformation already has been observed in previous simulations of rather small grains, up to 12 nm; however, the results have not been analyzed to distinguish small-scale grain-boundary sliding from bulk-mediated processes [100, 101]. In the more recent study of columnar grains up to 70 nm, it is shown that the dislocation splitting distance depends not only on the stacking-fault energy, but also on the resolved stress for nucleation [98]. It seems clear that the mechanical properties of nanocrystalline materials will have significant variations with grain size.

2.4. POINT DEFECTS

Point defects, including vacancies, self-interstitials and impurities, and their interaction with dislocations and grain boundaries, can have an important impact on the mechanical properties of metals. In elemental metals under high strain-rate conditions, for example, vacancies and self-interstitials are naturally created as part of the debris field left behind by moving dislocations, debris which will be encountered by other moving dislocations. An important validation test of interatomic potentials in elemental bcc metals such as Mo or Ta is thus the calculation of fully relaxed vacancy and self-interstitial formation and migration energies. These quantities together with formation volumes and migration paths have been studied in the context of MGPT potentials for both Mo and Ta [8, 12, 79]. In the case of Mo, the 1994 MGPT potentials [38] yield accurate relaxed vacancy formation and migration energies [8]. These potentials were also used to determine the lowest-energy self-interstitial configuration and the most favorable self-interstitial migration path. The former is the (110) split-dumbbell

configuration, while the latter is the so-called jump-and-rotation path along $\langle 111 \rangle$ directions. Subsequent first-principles DFT electronic-structure calculations have also been performed on the vacancy and self-interstitial formation and migration energies in both Mo and Ta [12, 40, 79]. In Mo, these calculations reveal that the $\langle 110 \rangle$ split-dumbbell self-interstitial formation energy and $\langle 111 \rangle$ jump-and-rotation migration energy are significantly overestimated with the 1994 MGPT potentials. Both of these problems are now corrected, however, with the new optimized Mo potentials [79, 102]. Similarly, the optimized Ta MGPT potentials have been used to calculate relaxed vacancy and self-interstitial formation energies and volumes, as well as migration energies [12]. Overall, there is very good agreement between theory and experiment and between DFT electronic-structure results and the MGPT results. In particular, the characteristic low vacancy migration energy of group-V metals like Ta is well predicted by the MGPT potentials.

2.5. RAPID RESOLIDIFICATION

Another important issue encountered at extreme conditions of pressure and temperature is that of the mechanical properties of new structural phases of a material created by fast dynamical processes (10^{-6} secs or faster). An example of such a process is the rapid resolidification of a molten metal like Ta though isentropic or isothermal compression to high pressure. The essential key to understanding and describing the mechanical properties in such an environment is identifying the underlying atomic- and micro-structural morphology of the resolidified material. Initial efforts to address the atomic structure question have focused on modeling rapid resolidification along both isobaric and isothermal loading paths in Ta, using large-scale MD simulations together with MGPT potentials [39, 103]. In such central transition metals, there is an energetically competitive phase with bcc, namely the low-symmetry, open-packed A15 structure, which is the well-known stable form of transition-metal-based superconductors such as Nb₃Sn. At ambient pressure, the A15 structure is known to occur as a metastable phase in W but has not as yet been experimentally observed in Ta. The MD/MGPT simulations on Ta demonstrate the existence of strong A15-bcc competition during the resolidification process and have revealed the first direct evidence of A15 ordering in the liquid prior to bcc crystallization [103]. Depending on the loading conditions, the final atomic structure of the resolidified solid is found to be either an amorphous glass state, with both A15 and bcc remnants, or a recyrstallized bcc solid. In the latter case, the A15-bcc competition acts as an effective kinetic barrier that delays the final bcc recrystallization by one or more orders of magnitude in time.

3. Linking length and time scales

In this section we discuss selected examples of recent atomistic research that directly impacts the issue of linking of length and/or time scales, as required in multiscale materials modeling.

3.1. QUANTUM-BASED INTERATOMIC POTENTIALS

A very fundamental linkage of length scales is that between first-principles DFT quantum mechanics, where at most a few hundred or so atoms can be treated accurately, and large-scale atomistic simulations, where one envisages thousands and even millions of atoms being simulated. The ultimate goal of both the GPT and BOP approaches is to encode, through systematic coarse graining of the underlying electronic structure, the necessary DFT quantum

mechanics into quantum-based interatomic potentials that can be used to determine accurate energies and forces in such simulations.

3.1.1. Generalized pseudopotential theory

Within the framework of DFT quantum mechanics, generalized pseudopotential theory (GPT) provides a fundamental basis for *ab initio* interatomic potentials in elemental simple and transition metals [29]. In the GPT applied to transition metals, a mixed wavefunction basis set of plane waves and localized *d* states is used to expand the electron density and total energy of the metal in terms of weak *sp* pseudopotential, *sp-d* hybridization, and *d-d* tight-binding-like matrix elements. In a real-space formulation, the derived interatomic potentials become well-defined functionals of these matrix elements and all quantities can be evaluated directly from first-principles without any external input. For an elemental bulk metal, the GPT provides a rigorous expansion of the total energy in the form a collective volume term plus sums over transferable, but volume dependent, two-, three-, four- and higher multi-ion interatomic potentials. To perform both efficient and accurate atomistic simulations with GPT potentials, one normally terminates the total-energy expansion at the lowest order that is consistent with the physics one seeks to describe. For systems where directional bonding is unimportant, such as series-end fcc metals, only the volume and pair-potential terms are retained. In this case, full atomistic simulations can be carried out directly using the *ab initio* GPT potentials without further approximation [45, 104].

For bcc transition metals, on the other hand, the angular-force, multi-ion potentials reflect directional bonding contributions from partially-filled *d* bands and are generally important to structural and mechanical properties. At the same time, however, in the full GPT these potentials are multidimensional functions that cannot be readily tabulated for application purposes. This has led to the development of the model GPT or MGPT for bcc transition metals [37, 38]. Within the MGPT, the multi-ion potentials are systematically approximated to achieve analytic forms that can then be readily applied to large-scale static and dynamic simulations. To compensate for the approximations introduced into the MGPT, a limited amount of parameterization is allowed in which the volume-dependent coefficients of the modeled potential contributions are constrained by experimental or *ab initio* theoretical data on basic bulk properties. In this form, the MGPT indeed provides a robust framework for performing accurate and predictive atomistic simulations on bulk transition metals. The original MGPT parameterization schemes for bcc metals, first developed for Mo [37, 38] have recently been generalized and greatly improved, with detailed application to the case of Ta [12, 39]. Very reliable Ta potentials have been so generated over a wide volume range and extending up to 1000 GPa in pressure. Many specific validation tests of the Ta potentials have been performed using accurate experimental data as well as the results of DFT electronic-structure calculations [12, 39]. The 1994 Mo potentials have also been widely used for bcc dislocation, grain-boundary and other defect calculations [8, 9, 19, 22, 65, 105, 106], although from the current perspective these potentials are probably less robust than the new Ta potentials. In this regard, a new set of Mo MGPT potentials, optimized to the same level as the Ta potentials, has recently been developed [102] and is now being applied to dislocation and defect calculations [13, 79], as discussed above.

3.1.2. Bond-order potentials

Bond-order potentials (BOPs) are a semi-empirical, real-space, linear-scaling tight-binding (TB) scheme for the description of atomic interactions. The theoretical basis for this approach has been developed by Pettifor and co-workers [31, 35, 36, 107–110]. Construction of BOPs follows the philosophy of parametrized TB theory with parameters fitted to reproduce basic equilibrium properties of the material studied as well as certain quantities determined using *ab initio* DFT-based calculations. Within this framework, the cohesive energy of a material consists of three parts written as

$$E_{\text{coh}} = E_{\text{bond}} + E_{\text{pair}} + E_{\text{env}}. \quad (2)$$

E_{bond} is the quantum-mechanical bond energy arising from the formation of the valence bands and for transition metals it is assumed to originate from the d electrons. E_{pair} is the repulsive pair-potential part of the energy that results from additional electrostatic interactions between the atoms and the overlap repulsion among the valence electrons. E_{env} is a remaining environmental part of the energy arising from the repulsion among the valence s and p electrons [111]. It is described by a central-force many body potential of the screened Yukawa form [112] and allows for exact fitting of the Cauchy pressures ($C_{12} - C_{44}$ in the cubic case).

An important feature of the construction of BOPs is that it is sequential. This means that first E_{bond} is constructed using solely the results of DFT-based calculations with no empirical input. Next E_{env} is obtained by fitting the Cauchy pressures and, finally, the pair-potential contribution E_{pair} is fitted so as to reproduce lattice parameter(s), remaining elastic moduli and the cohesive energy. The physically most important contribution to the cohesive energy is E_{bond} which comprises the main quantum-mechanical features of bonding, in particular the covalent character of the d bonding. Within the BOP formalism it is written as

$$E_{\text{bond}} = \sum_{\substack{I,J \\ i,j}} H_{I,J} \Theta_{J,I}, \quad (3)$$

where $H_{I,J}$ and $\Theta_{J,I}$ are the Hamiltonian and bond-order matrix elements, respectively. The index $I \equiv [i, L_i]$, where i numbers the atomic sites in the system studied and $L_i (= (\ell, m)_i)$, where ℓ denotes the quantum orbital moment and m the quantum magnetic moment for spherical symmetry. For a given Hamiltonian the bond-order matrix is expressed in terms of the derivatives of certain diagonal elements of the Green's function of the Schrödinger equation [107]. These diagonal elements are evaluated using the method of continued fractions and the Lanczos recursion algorithm [113]; in the present studies, four levels of continued fractions, i.e., nine moments of the density of states, have been used. The relatively complex procedures involved in the evaluation of E_{bond} are all part of the suit of computer codes available as the Order-N (OXON) package that is needed in all calculations employing BOPs. While the on-site Hamiltonian elements ($i = j$) do not enter directly into Eq. (3), they are needed when determining the bond order and are evaluated self-consistently to maintain local charge neutrality with respect to each atom. This condition reflects the perfect screening properties of metallic materials [114]. Finally, an important component of this package is evaluation of the derivatives of E_{bond} using the Hellmann-Feynman theorem. This is essential since atomistic simulations require not only evaluation of the energy but also forces acting on individual atoms.

In order to determine and examine the transferability of the bonding integrals $H_{I,J}$, they need to be evaluated as functions of the separation of atoms i and j for different structures. This

has been done via DFT-based calculations using the first-principles TB-LMTO method [115]. This method employs a small basis of atom-centered, short-range orbitals and the Hamiltonian has a simple analytical form that relates to a two-center, orthogonal TB Hamiltonian, so that a direct link with the TB-based BOP method can be established. For central transition metals such as Mo, the TB-LMTO $dd\sigma$ bonding integral shows good transferability among bcc, fcc and hcp structures and a unique dependence on the separation of atoms. However, the corresponding $dd\pi$ bond integral displays noticeably different values for the same atomic separation for different structures, as well as a discontinuity between the first and second nearest neighbors for the bcc structure. This is, presumably, the consequence of the proximity of the first and second neighbors in the bcc lattice, which results in different environmental screening for the two-center bond integrals. Hence, two-center bond integrals in an orthogonal TB scheme that are robust and transferable to different structures must be environment dependent. This has been recognized in recent years and a successful *ad hoc* scheme for introducing environmental dependence into bond integrals has been advanced [116]. Recently, we have developed an analytic form for the screening function that arises when a $d-d$ bond is screened by s electrons associated with neighboring atoms [117]. The derivation starts with a non-orthogonal two-center TB representation and transforms it to an effective orthogonal TB representation containing a screened Hamiltonian with an explicit screening function given in terms of the orbital overlap matrix. This screening function can be determined by applying the BOP theory and the Lanczos algorithm to the third level. Screened two-center bond integrals so determined for Mo, which are environment dependent, then reproduce excellently the TB-LMTO calculated values for both $dd\sigma$ and $dd\pi$ in Mo.

A basic test of the validity of the BOP potentials is comparison of energies of alternate structures relative to the bcc structure, specifically fcc, hcp, simple cubic and A15 structures. In all cases bcc is the lowest energy structure and the order of energies of alternate structures follows the trend found in DFT-based calculations. The study showing the success of the introduction of the environmental dependence into the bonding integrals has been the calculation of phonons in Mo. Without the environmental dependence the phonons near the N point were found to be much softer than what is suggested experimentally. The introduction of environmental screening leads to a substantial improvement of the calculated phonon spectrum. Most importantly, the transverse T2 mode phonon at the zone edge is very soft without screening and this improves significantly when the screening is introduced. Since the potentials are intended for atomistic modeling of extended defects, they also have to be applicable when the atomic environment is considerably different from that in the ideal lattice. While this can never be fully tested, a useful assessment can be made by investigating highly distorted structures encountered along certain deformation paths [118]. The most common path of this type is the Bain deformation path between the bcc and fcc lattices. However, results validated against DFT calculations for both Mo and Ta have also been obtained for a more complex trigonal path, which is also a deformation path between the bcc and fcc lattices but passing through the simple cubic structure [14, 119, 120].

3.2. DISLOCATION MOBILITY MODELS FOR DISLOCATION DYNAMICS

An important multiscale link between atomistic simulations and dislocation dynamics (DD) simulations of plasticity at the microscale is the mobility of individual dislocations. Dislocation mobility is currently being studied and modeled at the atomistic level using molecular statics, molecular dynamics and kinetic Monte Carlo simulations.

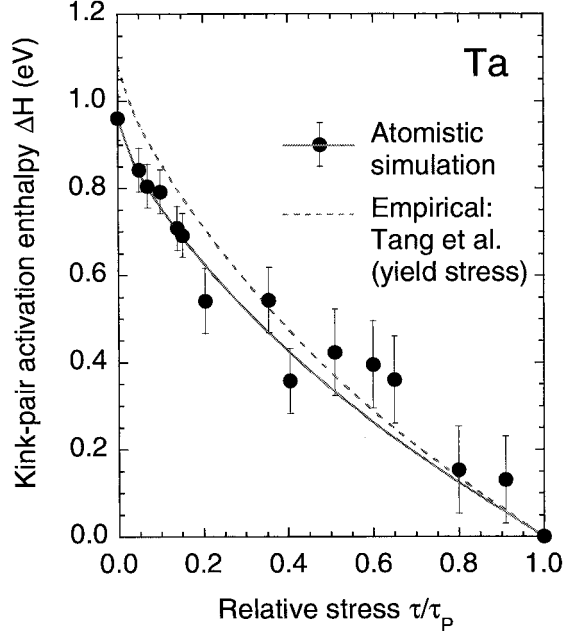


Figure 9. Kink-pair activation enthalpy as a function of relative applied stress for bcc Ta. The solid line is a fit to the calculated MGPT/GFBC atomistic data (solid points) [12, 13, 69] of the analytic form currently used in dislocation-dynamics simulations of single-crystal plasticity. The dashed line is the empirical result of Tang *et al.* [68] based on the observed yield stress.

3.2.1. Kink-pair activation enthalpy

In low-temperature DD simulations of bcc metals, it is assumed that the screw dislocation velocity is directly proportional to $\exp[-\Delta H(\tau/\tau_P)/k_B T]$, where $\Delta H(\tau/\tau_P)$ is the kink-pair activation enthalpy. The latter quantity is thus a key input parameter for defining dislocation mobility in such simulations. In the case of Ta, an analytic representation for $\Delta H(\tau/\tau_P)$ based on the atomistic MGPT/GFBC simulations discussed above has been developed and successfully implemented in DD simulations [12, 13, 69, 121] of single-crystal plasticity. This result is displayed in Fig. 9 and compared with the corresponding empirical result of Tang *et al.* [68] that reproduces the observed temperature dependence of the yield stress in Ta. This provides a first-generation atomistic-based dislocation mobility model for bcc Ta that has been successfully tested in DD simulations. This model also incorporates the basis for including the orientation dependence of the yield stress through the Peierls stress τ_P . In addition, this procedure of linking atomistic and DD simulations has now been extended to high pressure in Ta as well [121].

3.2.2. Kinetic Monte Carlo simulations

A useful approach to extend atomistic simulations of dislocation mobility to longer time scales is to treat the time evolution in the stochastic manner of Monte Carlo sampling. This has been carried through recently in a study of the intrinsic mobility of a dissociated dislocation in Si based on a kinetic Monte Carlo (kMC) treatment of kink nucleation, migration, and annihilation processes for a screw dislocation with full elastic interactions between the dissociated partials [122]. The kMC model is designed to produce the overall dislocation movement as the cumulative effects of a large number of such kink events, requiring for input only the

kink formation and migration energies that have been given by atomistic calculations. In this manner one can predict the response of dislocation velocity to a shear stress at temperature in the same length and time scales as the experiments, well beyond the range of large-scale molecular dynamics. It is found that good correspondence with the observed data is obtained with a set of kink activations energies rationally chosen from the various theoretical and experimental values that have been reported. The challenge of predicting experiments using purely calculated activation barriers by whatever method thus still remains to be met. On the other hand, by exploiting the ability to analyze correlated displacement of the leading and trailing partials, one finds a mechanistic explanation of the threshold stress effect, naturally resolving a long-standing postulate of ‘weak obstacles’ to kink propagation. More recently, the kMC model has been extended to screw dislocations in a bcc lattice by the incorporation of cross slip [123].

3.3. MODELING DEFECTS IN RADIATION DAMAGE

In a somewhat different context, modeling defect generation and transport in radiation damage in materials [124–126] provides further illustration of how one might bridge timescales from picoseconds to gigaseconds. In these problems, a database of the number and spatial distribution of defects produced in displacement cascades over picosecond timescales, obtained from MD simulations, provides atomistic input into kMC simulations of the longer time ($t \gg$ seconds) damage accumulation, along with information about the character and energetics of vacancy and self-interstitial clusters. Different kMC methods have recently been applied to predict the formation of sub-nanometer vacancy-solute clusters partially responsible for the embrittlement of reactor pressure vessel steels [124, 127, 128] and the accumulation of defect clusters in Cu as a function of key irradiation variables [124, 126, 129]. These recent results are in good agreement with experimental observations. Future challenges in this area will revolve around extending the efficiency of the method to simulate larger materials systems to longer times, without wasting computational effort on short-time physical processes that do not contribute to the long-time evolution.

3.4. NON-SCHMID EFFECTS FOR PLASTICITY THEORY

The dependence of the CRSS on χ for single screw dislocations in bcc metals discussed above, as well as other orientation dependencies revealed by atomistic studies (see for example, Ito and Vitek [59] and Yang *et al.* [12]), can be transferred into the macroscopic yield criteria for both single and polycrystals. These criteria then serve as a physical basis for constitutive relations employed in large-scale finite-element codes and/or hydrocodes. The recognition that it is the response of the dislocation core to external stresses, rather than the structure of the dislocation core in equilibrium, is essential for such transfer of atomic level information to the mesoscopic and macroscopic level to have a firm physical basis. For example, in the case of the CRSS vs χ dependence shown in Fig. 7 for Mo, as obtained with the FS potential, it has been concluded that the CRSS depends on shear stresses in two distinct {110} planes [130]. One of these is the Schmid stress in the glide plane of the {110} type and the other the shear stress in another {110} plane that is nearest to the {112} plane sheared in the twinning sense. The latter is a non-Schmid stress affecting the dislocation motion via the changes in the dislocation core. More complex non-Schmid effects may arise from shear stresses that act in the direction perpendicular to the Burgers vector, again via core transformations they induce

[59]. Effect of these stresses on the macroscopic plastic behavior can then be incorporated into the yield criteria similarly, if their influence is revealed in atomistic calculations.

3.5. ATOMISTIC MODELING FOR CONSTITUTIVE STRENGTH MODELS

Atomistic input can also be used directly to evaluate some of the parameters in existing constitutive strength models. One such example is the well-known Steinberg-Guinan strength model [131]. This model assumes that the yield stress of a macroscopic metal scales linearly with its (polycrystalline) average shear modulus G in the form

$$Y = Y_0 f(\varepsilon_p) G(P, T) / G_0, \quad (4)$$

where Y_0 and G_0 are normalization constants at ambient conditions and f is a bounded function of plastic strain ε_p , so that the entire pressure and temperature dependence of Y is carried by G . In addition, $G(P, T)$ itself is modeled in a simple way through its measured pressure and temperature derivatives at ambient conditions. It is here where accurate atomistic calculations can be used either to validate or, if necessary, to improve the model. In the case of bcc Ta, for example, the assumed pressure dependence of G is found to be reasonably consistent with first-principles calculations all the way to 1000 GPa [43]. In other cases, however, this may not be so, especially if one is modeling strength across phase boundaries.

Another direct approach to constitutive strength modeling has been undertaken by combining the micro-mechanical model of plasticity due to Stainier *et al.* [132], where controlling unit processes at the microscopic level are identified and modeled, with atomistic simulations, where fundamental defect nucleation and mobility parameters are determined by using force fields developed with the aid of quantum mechanical calculations of bond breaking [133]. For the case of the $a/2(111)$ screw dislocation in bcc Ta, the effective Peierls stress as a function of temperature, kink and anti-phase defect formation energies, and kink mobility were determined by MD simulations, and the parameters then used to calculate the stress-strain relations over a range of temperatures and strain rates. Figure 10 shows a comparison with experimental data of the model results on hardening, based on the parameters obtained by atomistic simulations. One may discern a number of common features in this comparison: variation of the initial yield with temperature, presence of a marked stage I of easy glide at low temperature, onset of parabolic stage II hardening, and temperature dependence of the saturation stress.

3.6. BOUNDARY CONDITIONS FOR COUPLED-DOMAIN SIMULATIONS

In the domain-decomposition approach to modeling defects, an atomistic region containing the defect(s) of interest is embedded in a surrounding medium treated using either a simpler interatomic interaction or a different set of degrees of freedom, such as finite elements. A general problem then arises in the spurious reflection of any elastic waves generated in the atomistic region from the domain boundary. Such effects are seen in, for example, the atomistic modeling of dislocation motion [134], crack propagation [135], and energetic particle-solid collisions [136]. In order to minimize such reflections, special boundary conditions have been proposed [137, 138], involving *ad hoc* viscous damping models. The empiricism turns out to be unnecessary, as shown recently by the introduction of a method that treats the interdomain interactions naturally through a memory function in the formalism of linear response theory [139]. This approach is effective in reducing phonon reflections at the domain

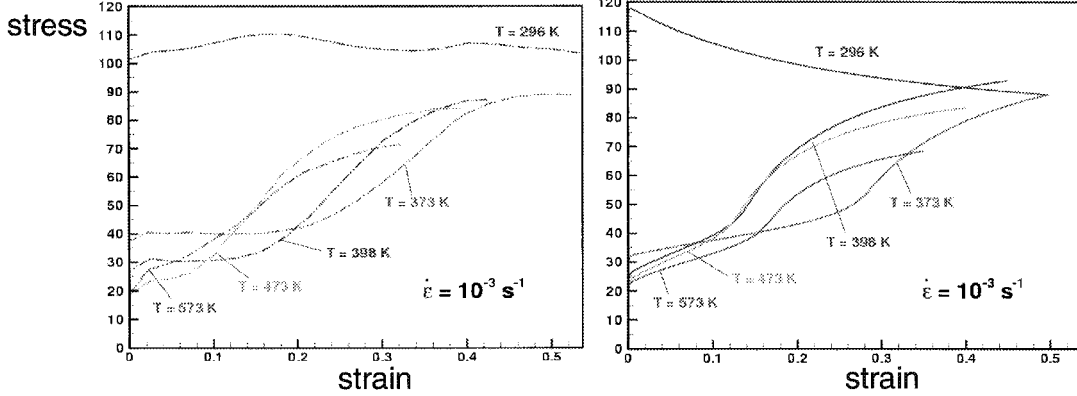


Figure 10. Temperature dependence of stress-strain curve for a [213] Ta single crystal at a strain rate of 10^{-3} . Left panel shows the experimental data, the right panel the predictions of the model with parameters from atomic-level simulations [133].

boundaries relative to existing methods, although it could be computational intensive since the time-dependent and particle-specific memory function matrix has to be evaluated numerically.

3.7. ACCELERATED MOLECULAR DYNAMICS

A bottleneck in the atomistic simulation of thermally activated processes is the time scale limitation of standard MD methods. While attempts to accelerate MD simulations have not as yet impacted double-kink dislocation processes and multiscale modeling in bcc metals, they have had success in certain surface and nanoscience problems. In the case of thin film growth by vapor deposition, MD is well suited to simulate the individual event of an atom impinging on the substrate, whereas it would be quite inadequate for describing the activated diffusion and reorganization events that occur during the milliseconds or seconds before the next atom deposition event. If the transition state (i.e., the saddle point) for a given diffusion pathway were known, transition state theory can be used to compute directly the rate constant. If all the possible events are known for a given system, these rate constants can be employed in a kMC algorithm to evolve the system from state to state over long time scales. For realistic systems, not only are the transition states often hard to determine, but also our intuition about how the system will behave is not good enough to always ensure that no key events are missing from the kMC treatment. For example, the dominant pathway for diffusive motion of an adatom on the simple Pt (100) surface is now known to be a concerted two-atom exchange mechanism, rather than a simple hop. For clusters of atoms, and complex geometries that arise during growth, even more complicated mechanisms have been observed.

Recently new methods have been developed to treat the problem of complex, infrequent-event processes. The idea is to directly accelerate the MD simulation to achieve longer times, rather than trying to specify in advance what the dominant mechanisms are. To do this, one takes advantage of the infrequent-event nature of the dynamics. One need not worry about whether the vibrational motion within the potential basin is correctly described, so long as the relative probability of escaping along a particular pathway is preserved. This is the essence of transition state theory, and the basis of three new methods: hyperdynamics [140, 141], temperature accelerated dynamics (TAD) [142], and parallel replica dynamics [143, 144]. These methods have been tested on various applications, and have had particular success in

the simulation of the film growth problem. For example, recently it has been possible to match experimental growth conditions (slower than a monolayer per second) for the vapor deposited growth of silver on Ag(100) using the TAD method [145]. At temperatures of 70 K and below, one observes a competition between thermally activated smoothing of the crystal surface and a surprisingly strong roughening due to steering of the deposited atoms as they approach the surface.

Another time scale problem is encountered in nanotechnology where continuum analysis becomes increasingly less reliable as the system size reduces below 100 nm. Diverse atomistic simulation methods and structure optimization simulations are currently being applied to investigate emerging nanostructured systems, e.g., fullerenes, nanotubes, nanoparticles, molecular devices, etc. Because the number of atoms in these systems is approaching the capability of current computers, for example, 30 nm Au nanoparticle contains less than a million atoms, and there are 10^4 – 10^7 carbon atoms in nanotubes of 1–10 nm diameter and 0.1–10 nm length, size or length scale is no longer an issue. On the other hand, bridging the time scale still remains a challenge in realistic modeling of dynamic behavior of nanomaterials. One such problem is the strength of carbon nanotubes under an external load. Several molecular static and dynamics simulations had previously given a prediction of 15–25% yield strain, corresponding to a yield stress of 200–350 GPa [146, 147]. More recent MD simulations with systematic strain rate and temperature effects show that finite temperature effect significantly reduces the yield strain down to 5–6%, while the strain rate is still very high compared to typical experimental conditions [148].

To overcome the time scale problem of high strain rates, a scheme has been formulated to use high temperature to effectively accelerate the time scale with a relationship of the form: $\text{strain} = A + B(T) \ln(\text{strain rate})$ [148]. MD simulations have been run with different strain rates and temperatures over ranges of 10^7 – 10^9 and 300–2400 K, respectively. This relationship is well satisfied for nanotube plastic yielding under tensile stress, but compressive stress does not produce the expected behavior. From the detailed analysis of the nanotube structure evolution under the compressive stress, it is found that the wavelength geometric instability strongly depends on the strain rate and that the geometric deformation initiates the plastic yield response of the nanotube. Consequently, the nanotubes under compression exhibit complex interaction between activated plastic response and configuration fluctuations leading to a fundamental time scale problem in simulating their mechanical responses. This example represents a common behavior of nanomaterial systems as opposed to an exceptional case. Many nanomaterials, e.g., polymers, proteins, DNA, RNA, molecular wires, etc., show characteristic slow modes associated with configuration fluctuations, which are quite different from rare events of chemical bond breaking. These slow modes and their complex interactions with rare events make the time scale problem the most significant roadblock in applying atomistic simulations to nanomaterials study.

4. Experimental validation

In this section we discuss a few selected recent and current experimental efforts that provide complementary and validating data for the atomistic simulations.

4.1. HIGH-PRESSURE ELASTIC MODULI

A number of different experimental methods exist to investigate the elastic moduli of solids, although the conventional ones have significant limitations with respect to material type and pressure. Standard ultrasonic techniques, for example, require a single crystal to measure the individual moduli C_{ij} and are applicable only at low pressure. In addition, experimental methods using acoustic scattering of light to measure elastic moduli are usually limited to transparent, single-crystals at moderate pressure and are not applicable to opaque metals or to polycrystalline materials. On the other hand, synchrotron x-ray diffraction combined with a diamond-anvil cell (DAC) is capable of measuring the bulk modulus of solids to very high pressures and temperatures under hydrostatic loading conditions. To obtain information about the shear moduli and yield strength, such techniques have now been extended to non-hydrostatic, uniaxial compression [44, 149]. Under uniaxial compression, the usual circular powder diffraction patterns obtained in the DAC with hydrostatic loading become elliptically distorted due to the different stress components acting on the randomly oriented lattice planes. The elliptical distortion, defined by the ratio of the lattice-plane spacing measured under non-hydrostatic and hydrostatic conditions, is then a measurable function of the angle between the diffracting plane and the uniaxial compression axis. From this information the individual single-crystal moduli $C_{ij}(P)$ can be determined. Another new DAC technique [150] uses impulsive stimulated light scattering (ISLS) to measure surface acoustic wave velocities under pressure in single or poly crystals, from which elastic moduli can be determined. Unlike conventional acoustic scattering methods, this technique is applicable to opaque metals.

Singh *et al.* have used a non-hydrostatic stress technique in the DAC together with energy-dispersive x-ray diffraction on polycrystalline samples to estimate the single-crystal elastic moduli of hcp Fe to 200 GPa [149], fcc Au and hcp Re to 37 GPa [151], and bcc Mo to 24 GPa [152]. Cynn and Yoo have recently developed a closely related high-pressure DAC technique called SAX (Stress- and Angle-resolved X-ray diffraction) to probe the shear modulus and yield strength in polycrystalline materials [44]. They have similarly determined the single-crystal elastic moduli of bcc Ta to 105 GPa, as shown above in Fig. 1. Crowhurst *et al.* [150, 153] have used their ISLS technique to measure the polycrystalline elastic moduli of Ta to 40 GPa.

4.2. HREM IMAGING OF DISLOCATION AND GRAIN-BOUNDARY ATOMIC STRUCTURES

The atomic structures of dislocation cores in bcc metals are quite compact when compared to fcc metals, which often have dissociation of dislocations into partials with an associated stacking fault. This compact core has led to experimental difficulties in fully characterizing the core structure of the screw dislocation in bcc metals [154], as compared to the successes in fcc metals and intermetallic systems [155–157]. However, comparison of the atomic neighborhood of a dislocation core with that of a grain boundary often reveal that they are much the same. Therefore a validation experiment designed around grain boundary atomic structure should provide much the same confidence in the atomistic modeling technique. Additionally, the experimental characterization of the atomic structure of grain boundaries is a much more straightforward process. A number of recent HREM experimental grain-boundary characterizations of bcc metals have been reported [17–20, 158].

One of the important goals of several of these investigations into the grain-boundary structure in bcc metals has been the validation of the quantum-based interatomic potentials that

incorporate angularly dependent interactions. As discussed above, there has been close agreement between the predictions of the atomistic simulations with these potentials and the results of experimental observations of the $\Sigma 5$ (310)/[001] symmetric tilt grain boundary in Nb, Mo, and Ta [17, 19, 20]. The quantitative feature of particular interest in this boundary is the state of rigid-body displacement between the grains on either side of the boundary. Explicit methods have been developed for quantitative analysis of this shift by HREM for comparison with theoretical predictions [23], which has revealed the good agreement between theory and experiment.

4.3. NANOINDENTATION EXPERIMENTS

Nanoindentation permits the study of plasticity of materials in very small volumes, from the atomic scale, through the micro- and meso-scales to the continuum scale. As such, it provides a particularly good tool for validating the predictions of multiscale modeling and simulation of material behavior. In this approach, one can consider the nucleation of dislocations in perfect crystals, as well as the effects of grain boundary proximity, on the initiation of plasticity.

Nanoindentation of Mo and Ta epitaxial films and polycrystalline Au thin films at the nanometer depth scale reveals irregular load-displacement curves that are associated with the nucleation of dislocations [159–161]. The shear stresses at which the first inelastic events are triggered compare favorably with estimates of the theoretical shear strengths of perfect crystals. In these experiments, a diamond indenter with a slightly rounded tip (radius about 50–100 nm) is pushed into the surface of a crystal. Initially one sees a Hertzian elastic loading behavior. The load-displacement curve for the Au polycrystal shows reversible loading and unloading behavior. This is purely elastic behavior. In each case an abrupt displacement burst occurs at a critical load. This corresponds to the nucleation of dislocations – a nanoscale deformation effect. The resolved shear stresses needed to produce these irreversible displacements are very high – they correspond to the theoretical strength of the crystal. What makes these experiments especially interesting is that the largest shear stresses are found not at the surface but beneath the surface. As a consequence, the nucleation of dislocations occurs within the crystal and is not affected by imperfections at the surface of the crystal. Also, in these small-scale indentations there are no dislocations under the indenter (the dislocation density is too low and the indentation area is too small) with the consequence that the deformation of initially perfect crystals can be studied. These are the most ideal conditions for deformation, conditions that can be treated with various kinds of atomistic modeling schemes.

In an effort to link these experimental results to atomistic phenomena, MD modeling of nanometer scale indentations in Au bicrystals has been done [160, 161]. The MD simulations show that discrete plastic events are associated with the nucleation of dislocations beneath the surface and that grain boundaries can facilitate the dislocation nucleation process. The MD simulations show both Hertzian elastic and discrete plastic deformation. In spite of the small size of the systems being considered in these simulations, the load displacement response is very much like the experiments. One finds Hertzian elastic loading up to a depth of about 4 Å. Then a small discrete load drop is observed. At larger displacements, still larger load drops are observed. The abrupt load drops are associated with dislocation nucleation under the indenter tip. In the simulations the indenter displacement is prescribed, so that the system acts as a hard testing system. By contrast, in the experiments one has a soft testing system and displacement discontinuities are observed instead of load drops. The initial loading curve is well described by the Hertz theory. After several load drops, the indenter is withdrawn from the sample.

The corresponding unloading curve is analyzed according to the Sneddon theory of elastic contact (used in experimental nanoindentation studies). The elastic modulus extracted from that analysis gives a result that is in good agreement with the bulk elastic properties of Au.

5. Concluding remarks

We believe that the research discussed in the present paper is representative of current atomistic simulation work contributing to the multiscale modeling of plasticity and strength. To the work cited, no doubt could be added many other additional examples, especially in non-bcc materials. It is clear that atomistic simulations for multiscale modeling of plasticity and strength are now moving into an advanced phase, where not only are generic mechanisms in simple systems being addressed but also where quantum-based predictions for real complex materials at both ambient and extreme conditions are being made. The forefront challenge for the future is to firmly establish all relevant fundamental linkages, both in length scale and in time scale, with micro-, meso- and continuum descriptions of plasticity and strength.

Acknowledgements

This work was performed in part under the auspices of the U.S. Department of Energy by the University of California Lawrence Livermore National Laboratory under contract number W-7405-ENG-48. The authors wish to thank all of the participants of the Bodega Bay Workshop who contributed either directly or indirectly to the work reviewed in this paper. In particular, the authors would like to acknowledge the contributions of Drs Tomas Arias, Tagin Cagin, Wei Cai, Geoff Campbell, Jinpeng Chang, Kyeongjae Cho, Bruce Clemens, Hyunchae Cynn, Maurice de Koning, Tim Germann, William Goddard III, Wayne King, Dave Lassila, Ju Li, Bill Morris, Bill Nix, David Pettifor, Per Söderlind, Fred Streitz, Meijie Tang, Brian Wirth, Chris Woodward, and Lin Yang.

References

1. Bulatov, V.V., J. of Computer-Aided Mater. Design, (2003), this issue.
2. Becker, R. and Stolken, J., J. of Computer-Aided Mater. Design, (2003), this issue.
3. See, for example, Mailhoit, C. and Yip, S. (Eds.) J. of Computer-Aided Mater. Design, 5 (1998), special issue devoted to ASCI materials modeling.
4. Vitek, V., Crystal Lattice Defects, 5 (1974) 1.
5. Duesbery, M.S. and Vitek, V., Acta Mater., 46 (1998) 1481.
6. Duesbery, M.S., Proc. R. Soc. Lond., A392 (1984) 175.
7. Duesbery, M.S. and Basinski, Z.S., Acta Metall. Mater., 41 (1993) 643.
8. Xu, W. and Moriarty, J.A., Phys. Rev., B54 (1996) 6941.
9. Rao, S. and Woodward, C., Philos. Mag., A81 (2001) 1317.
10. Ismail-Beigi, S. and Arias, T.A., Phys. Rev. Lett., 84 (2000) 1499.
11. Woodward, C. and Rao, S.I., Philos. Mag., A81 (2001) 1305.
12. Yang, L.H., Söderlind, P. and Moriarty, J.A., Philos. Mag., A81 (2001) 1355.
13. Yang, L.H., Söderlind, P. and Moriarty, J.A., to be published.
14. Mrovec, M., Ph.D. Thesis, University of Pennsylvania (2002).
15. Vitek, V., Philos. Mag., (2003), to be published.
16. Sadigh, B., Cai, W. and Bulatov, V.V., unpublished.
17. Campbell, G.H., Foiles, S.M., Gumbsch, P., Rühle, M. and King, W.E., Phys. Rev. Lett., 70 (1993) 449.
18. Bacia, M., Morillo, J., Pénisson, J.-M. and Pontikis, V., Philos. Mag., A76 (1997) 945.

19. Campbell, G.H., Belak, J. and Moriarty, J.A., *Acta Mater.*, 47 (1999) 3977.
20. Campbell, G.H., Belak, J. and Moriarty, J.A., *Scripta Mater.*, 43 (2000) 659.
21. Ochs, T., Beck, O., Elsässer, C. and Meyer, B., *Philos. Mag.*, A80 (2000) 351.
22. Ochs, T., Elsässer, C., Mrovec, M., Vítek, V., Belak, J. and Moriarty, J.A., *Philos. Mag.*, A80 (2000) 2405.
23. Campbell, G.H., Kumar, M., King, W.E., Belak, J., Moriarty, J.A. and Foiles, S.M., *Philos. Mag.*, A82(2002) 1573.
24. Rao S., Hernandez C., Simmons J., Parthasarathy T. and Woodward C., *Philos. Mag.*, A77 (1998) 231.
25. Rao, S., Parthasarathy, T.A. and Woodward, C., *Philos. Mag.*, A79 (1999) 1167.
26. Cai, W., Bulatov, V., Chang, J., Li, J. and Yip, S., *Phys. Rev. Lett.*, 86 (2001) 5727.
27. Daw, M. and Baskes, M., *Phys. Rev. Lett.*, 50 (1983) 1285 and *Phys. Rev.*, B29 (1984) 6443; Daw, M., Foiles, S.M. and Baskes, M., *Mater. Sci. Rep.*, 9 (1993) 251.
28. Finnis, M.W. and Sinclair, J.E., *Philos. Mag.*, A50 (1984) 45; Ackland, G.J. and Thetford, R., *Philos. Mag.*, A56 (1987) 15; Ackland, G.J. and Vitek, V., *Phys. Rev.*, B41 (1990) 10324.
29. Moriarty, J.A., *Phys. Rev.*, B38 (1988) 3199.
30. Carlsson, A., In Seitz, F., Turnbull, D. and Ehrenreich, H. (Eds.) *Solid State Physics*, Vol 43, Academic Press, New York, NY, 1990, p. 1.
31. Pettifor, D.G., *Phys. Rev. Lett.*, 63 (1989) 2480.
32. Carlsson, A., *Phys. Rev.*, B44 (1991) 6590.
33. Foiles, S.M., *Phys. Rev.*, B48 (1993) 4287.
34. Hohenberg, P. and Kohn, W., *Phys. Rev.*, 136 (1964) B864; Kohn, W. and Sham, L., *Phys. Rev.*, 140 (1965) A1133.
35. Pettifor, D.G., Aoki, M., Gumbsch, P., Horsfield, A.P., Nguyen-Manh, D. and Vitek, V., *Mater. Sci. Eng.*, A192-193 (1995) 24.
36. Pettifor, D.G., Oleinik, I.I., Nguyen-Manh, D. and Vitek, V., *Computational Mater. Sci.*, 23 (2002) 33.
37. Moriarty, J.A., *Phys. Rev.*, B42 (1990) 1609.
38. Moriarty, J.A., *Phys. Rev.*, B49 (1994) 12431.
39. Moriarty, J.A., Belak, J.F., Rudd, R.E., Söderlind, P., Streitz, F.H. and Yang, L.H., *J. Phys.: Condens. Matter*, 14 (2002) 2825.
40. Söderlind, P., Yang, L.H., Moriarty, J.A. and Wills, J.M., *Phys. Rev.*, B61 (2000) 2579.
41. Woodward, C. and Rao, S.I., *Phys. Rev. Lett.*, 88 (2002) 216402.
42. Katahara, K.W., Manghnani, M.H. and Fisher, E.S., *J. Phys. F: Metal Phys.*, 9 (1979) 773.
43. Söderlind, P. and Moriarty, J.A., *Phys. Rev.*, B57 (1998) 10340.
44. Cynn, H. and Yoo, C.-S., to be published.
45. Greeff, C.W. and Moriarty, J.A., *Phys. Rev.*, B59 (1999) 3427.
46. Gülsen, O. and Cohen, R.E., *Phys. Rev.*, B65 (2002) 64103.
47. Orlowski, D., Söderlind, P. and Moriarty, J.A., to be published.
48. Born, M., *Proc. Cambridge Philos. Soc.*, 36 (1940) 160.
49. Hill, R., *Math. Proc. Camb. Philos. Soc.*, 77 (1975) 225.
50. Hill, R. and Milstein, F., *Phys. Rev.*, B15 (1977) 3087.
51. Kelly, A. and Macmillan, N.H., *Strong Solids*, Clarendon, Oxford, 1986.
52. Wallace, D.C., *Thermodynamics of Crystals*, Wiley, New York, 1972.
53. Wang, J., Li, J., Yip, S., Phillipot, S. and Wolf, D., *Phys. Rev.*, B52 (1995) 12627.
54. Morris Jr., J.W. and Krenn, C.R., *Philos. Mag.*, A80 (2000) 2827.
55. Li, J., Ph.D. Thesis, MIT, 2000.
56. Paxton, A.T., Gumbsch, P. and Methfessel, M., *Philos. Mag. Lett.*, 63 (1991) 267.
57. Morris Jr., J.W., Krenn, C.R., Roundy, D. and Cohen, M.L., In Turchi, P.E. and Gonis, A. (Eds.) *Phase Transformations and Evolution in Materials*, TMS, Warrendale, PA, 2000, p. 187.
58. Roundy, D., Krenn, C.R., Cohen, M.L. and Morris Jr., J.W., *Philos. Mag.*, A81 (2001) 1725.
59. Ito, K. and Vitek, V., *Philos. Mag.*, A81 (2001) 1387.
60. Vitek, V., Perrin, R.C. and Bowen, D.K., *Philos. Mag.* A21 (1970) 1049.
61. Basinski, Z.S., Duesbery, M.S. and Taylor, R., *Can. J. Phys.*, 49 (1971) 2160.
62. Cai, W., Ph.D. Thesis, MIT (2001).
63. Yamaguchi, M. and Vitek, V., *J. Phys. F: Metal Phys.*, 3 (1973) 523.
64. Duesbery, M.S., *Acta Metall.*, 31 (1983) 1747 and 1759.
65. Xu, W. and Moriarty, J.A., *Comput. Mater. Sci.*, 9 (1998) 348.

66. Duesbery, M.S., private communication.
67. Seeger, A. and Hollang, L., Materials Transactions JIM, 41 (2000) 141; Hollang, L., Hommel, M. and Seeger, A., Phys. Stat. Sol., (a) 160, (1997) 329.
68. Tang M., Kubin, L.P. and Canova, G.R., Acta Mater., 46 (1998) 3221; Tang, M., private communicaton.
69. Yang, L.H., Tang, M. and Moriarty, J.A., Mat. Res. Soc. Symp. Proc., 653 (2001) Z1.2.1.
70. Edagawa, K., Suzuki, T. and Takeuchi, S., Phys. Rev., B55 (1997) 6180.
71. Christian, J.W., Metall. Trans., A14 (1983) 1237.
72. Vitek, V., In Lorretto, M. (Ed.)Dislocations and Properties of Real Materials, The Institute of Metals, London, 1985, p. 30.
73. Duesbery, M.S., In Nabarro, F.R.N. (Ed.) Dislocations in Solids, Vol. 8, North Holland, Amsterdam, 1989, p. 67.
74. Duesbery, M.S. and Richardson, G.Y., CRC Critical Reviews in Solid State and Materials Science, 17 (1991) 1.
75. Vitek, V., Prog. Mater. Sci., 36 (1992) 1.
76. Susuki, T., Kamimura, Y. and Kirchner, H.O.K., Philos. Mag., A79 (1999) 1629 and references therein.
77. Lachenmann, R. and Schultz, H., Scripta Met., 4 (1970) 709.
78. Duesbery, M.S. and Xu W., Scripta Mater., 39 (1998) 283.
79. Yang, L.H., private communication.
80. Bulatov, V.V., Cai, W. and Krenn, C., unpublished.
81. Duesbery, M.S., Michel and D.J., Joos, B., Phys. Rev., B43 (1991) 5143.
82. Bulatov, V.V., Yip, S. and Argon, A.S., Philos. Mag., A72 (1995) 453.
83. Ren, Q., Joos, B. and Duesbery, M.S., Phys. Rev., B52 (1995) 13223.
84. Koizumi, H., Kamimura, Y. and Suzuki, T., Philos. Mag., A80 (2000) 609.
85. Chang, J., Bulatov, V. and Yip, S., J. Computer-Aided Mater. Design, 6 (1999) 165.
86. Chang, J., Cai, W., Bulatov, V.V. and Yip, S., Mater. Sci. Eng., A309-310 (2001) 160.
87. Rodney, D. and Martin, G., Phys. Rev. Lett., 82 (1999) 3272.
88. Chang, J., Ph.D. Thesis, MIT (2003), and to be published.
89. Wolfer, W.G., Phonon Drag on Dislocations at High Pressures, LLNL Report UCRL-ID-136221 (1999).
90. Bulatov, V.V. and Cai, W., Phys. Rev. Lett., 89 (2002) 115501.
91. Garratt-Reed, A.J. and Taylor, G., Philos. Mag., A39 (1979) 597.
92. Lassila, D.H. and Hsiung, L., private communication.
93. DeHosson, J.T.M., Pestman, B.J. and Vitek, V., In Baker, I., Darolia, R., and Whittenberger, J.D. and Yoo, M.H. (Eds.) High-Temperature Ordered Intermetallic Alloys V, Vol. 288, Materials Research Society, Pittsburgh, 1993, p. 299.
94. Pestman, B.J., DeHosson, J.T.M., Vitek, V. and Schapink, F.W., J. Phys. France, 51 (1990) C1-311.
95. Pestman, B.J., DeHosson, J.T.M., Vitek, V. and Schapink, F.W., Philos. Mag., A64 (1991) 951.
96. Miller, R. and Abraham, F., unpublished and private communication.
97. de Koning, M., Miller, R., Bulatov, V.V. and Abraham, F., Philos. Mag., A82 (2002) 2511.
98. Yamakov, V., Wolf, D., Salazar, M., Phillpot, S.R. and Gleiter, H., Acta Mater., 49 (2001) 2713.
99. Cottrell, A.H., Dislocations and Plastic Flow in Crystals, Clarendon Press, Oxford, 1961.
100. Schiotz, J., Di Tolla, F.D. and Jacobsen, K.W., Phys. Rev., B60 (1999) 11971.
101. Swygenhoven, H.V., Spaczer and M., Caro, A., Acta Mater., 47 (1999) 3117.
102. Moriarty, J.A., unpublished.
103. Streitz, F.H. and Moriarty, J.A., to be published.
104. Moriarty, J.A. and Althoff, J.D., Phys. Rev., B51 (1995) 5609.
105. Yesilletn, D. and Arias, T.A., Phys. Rev., B64 (2001) 174101.
106. Bulatov, V.V., Justo, J.F., Cai, W. and Yip, S., Phys. Rev. Lett., 79 (1997) 5042.
107. Horsfield, A.P., Bratkovsky, A.M., Fearn, M., Pettifor, D.G. and Aoki, M., Phys. Rev., B53 (1996) 12694 and Horsfield, A.P., Bratkovsky, A.M., Pettifor, D.G. and Aoki, M., Phys. Rev., B53 (1996) 1656.
108. Aoki, M., Horsfield, A.P. and Pettifor, D.G., J Phase Equilib., 18 (1997) 614.
109. Bowler, D.R., Aoki, M., Gorringe, C.M., Horsfield, A.P. and Pettifor, D.G., Modelling and Simulation in Mater. Sci. Eng., 5 (1997) 199.
110. Znam, S., Nguyen-Manh, D., Pettifor, D.G. and Vitek, V., Philos. Mag., A83 (2003) 99.
111. Pettifor, D.G., J.Phys. F: Metal Phys., 8 (1978) 219.

112. Nguyen-Manh, D., Pettifor, D.G., Znam, S. and Vitek, V., In Turchi, P.E.A., Gonis, A. and Colombo, L. (Eds.) Tight-Binding Approach to Computational Materials Science, Vol. 491, Materials Research Society, Pittsburgh, 1998, p. 353.
113. Lanczos, C., J. Res. Natl. Bur. Stand., 45 (1950) 225.
114. Pettifor, D.G., Bonding and Structure of Molecules and Solids, Oxford University Press, Oxford, 1995.
115. Andersen, O.K., Jepsen, O. and Glötzel, D., In Bassani, F., Fumi, F. and Tosi, M.P. (Eds.) Highlights of Condensed Matter Theory, North Holland, Amsterdam 1985, p. 59.
116. Haas, H., Wang, C.Z., Fähnle, M., Elsässer, C. and Ho, K.M., Phys. Rev., B57, (1998) 1461.
117. Nguyen-Manh, D., Pettifor, D.G. and Vitek, V., Phys. Rev. Lett., 85 (2000) 4136.
118. Paidar, V., Wang, L.G., Sob, M. and Vitek, V., Modelling and Simulation in Mat. Sci. Eng., 7 (1999) 369.
119. Mrovec, M., Vitek, V., Nguyen-Manh, D., Pettifor, D.G., Wang, L.G. and Sob, M., In Bulatov, V., Diaz de la Rubia, T., Phillips, R., Kaxiras, E. and Ghoniem, N. (Eds.) Multiscale Modeling of Materials, Vol. 538, Materials Research Society, Pittsburgh, 1999, p. 529.
120. Mrovec, M., Vitek, V., Nguyen-Manh, D., Pettifor, D.G., Wang, L.G. and Sob, M., In Robertson, I.M., Lassila, D.H., Devincre, B. and Phillips, R. (Eds.) Vol. 578, Materials Research Society, Pittsburgh, 2000, p. 199.
121. Tang, M., private communication.
122. Cai, W., de Koning, M., Bulatov, V.V. and Yip, S., Phys. Rev. Lett., 85 (2000) 3213.
123. Cai, W., Bulatov, V.V., Yip, S. and Argon, A.S., Mater. Sci. Eng., A309-310 (2001) 270.
124. Odette, G.R., Wirth, B.D., Bacon, D.J. and Ghoniem, N.M., MRS Bulletin 26 (2001) 176.
125. Wirth, B.D., Caturla, M.J., Diaz de la Rubia, T., Khraishi, T. and Zbib, H., Nuc. Instruments and Methods, B180 (2001) 23.
126. Caturla, M.J., Soneda, N., Alonso, E., Wirth, B.D., Diaz de la Rubia, T. and M. Perlado, J., J. Nuc. Mat., 276 (2000) 13.
127. Wirth, B.D. and Odette, G.R., MRS Symp. Proc., 540 (1999) 637.
128. Domain, C., Beequart, C.S. and Van Duyse, J.C., MRS Symp. Proc., 540 (1999) 643.
129. Xu, Q., Heinisch, H.L. and Yoshiie, T., J. of Computer-Aided Mater. Design, 6 (1999) 215.
130. Bassani, J.L., Ito, K. and Vitek, V., Mat. Sci. Eng., A319 (2001) 97.
131. Steinberg, D.J., Cochran, S.G., and Guinan, J. Appl. Phys., 51 (1980) 1498.
132. Stainier, L., Cuitino, A.M. and Ortiz, M., J. Mech. Phys. Solids, 50 (2002) 1511.
133. Cuitino, A.M., Stainier, L., Wang, G.F., Strachan, A., Cagin, T., Goddard, W.A. and Ortiz, M., J. Computer-Aided Mater. Design, 8 (2001) 127.
134. Ohsawa, K. and Kuramoto, E., J. Appl. Phys., 86 (1999) 179.
135. Abraham, F.F. and Gao, H., Phys. Rev. Lett., 84 (2000) 3113.
136. Carroll, S.J., Nellist, P.D., Palmer, R.E., Hobday, Smith, R., Phys. Rev. Lett., 84 (2000) 2654.
137. Gumbsch, P., Zhou, S.J., Holian, B.L., Phys. Rev., B55 (1997) 3445.
138. Moseler, M., Nordiek, J., Haberland, H., Phys. Rev., B56 (1997) 15439.
139. Cai, W., Bulatov, V.V., Justo, J.F., Argon, A.S. and Yip, S., Phys. Rev. Lett., 84 (2000) 3346.
140. Voter, A.F., J. Chem. Phys., 106 (1997) 4665.
141. Voter, A.F., Phys. Rev. Lett., 78 (1997) 3908.
142. Sorensen, M.R. and Voter, A.F., J. Chem. Phys., 112 (2000) 9599.
143. Voter, A.F., Phys. Rev., B57 (1998) 13985.
144. Voter, A.F. and Germann, T.C., Mat. Res. Soc. Symp. Proc., 528 (1998) 221.
145. Montalenti, F., Sorensen, M.R. and Voter, A.F., Phys. Rev. Lett., 87 (2001) 126101.
146. Yakobson, B.I., Brabec, C.J. and Bernholc, J., Phys. Rev. Lett., 76 (1996) 2511.
147. Nardelli, M.B., Yakobson, B.I. and Bernholc, J., Phys. Rev. Lett., 81 (1998) 4656.
148. Wei, C., Cho, K., and Srivastava, D., Mat. Res. Soc. Symp. Proc., 677 (2001), AA6.5.1
149. Singh, A.K., Mao, H.-K., Shu, J. and Hemley, R.J., Phys. Rev. Lett., 80 (1998) 2157.
150. Crowhurst, J.C., Abramson, E.H., Slutsky, L.J., Brown, J.M., Zaug, J.M. and Harrell, M. D., Phys. Rev., B64 (2001) 100103.
151. Duffy, T.S., Shen, G., Heinz, D.L., Shu, J., Ma, Y., Mao, H.-K., Hemley, R.J. and Singh, A.K., Phys. Rev., B60 (1999) 15063.
152. Duffy, T.S., Shen, G., Shu, J., Mao, H.-K., Hemley, R.J. and Singh, A.K., J., Appl. Phys., 86 (1999) 6729.
153. Crowhurst, J.C., private communication.
154. Sigle, W., Philos. Mag., A79 (1999) 1009.

155. Balk, T.J. and Hemker, K.J., *Philos. Mag.*, A81 (2001) 1507.
156. Baluc, N., Karthaler, H.P. and Mills, M.J., *Philos. Mag.*, A64 (1991) 137.
157. Mills, M.J. and Stadelmann, P., *Philos. Mag.*, A60 (1989) 355.
158. Vystavel, T., Penisson, J.M. and Gemperle, A., *Philos. Mag.*, A81 (2001) 417.
159. Nix, W.D. and Clemens, B.M., private communication.
160. Lilleodden, E.T., Zimmerman, J.A., Foiles, S.M. and Nix, W.D., *Mat. Res. Soc. Symp. Proc.*, 673 (2001) 1.3.1.
161. Lilleodden, E.T., Zimmerman, J.A., Foiles, S.M. and Nix, W.D., *J. Mech. Phys. Solids*, 51 (2003) 901.